Empirical Bayes evaluation of fused EEG-MEG source reconstruction: Application to auditory mismatch evoked responses

Françoise Lecaignard, Olivier Bertrand, Anne Caclin, Jérémie Mattout

Empirical Bayes evaluation of fused EEG-MEG source reconstruction: Application to auditory mismatch evoked responses

Françoise Lecaignard[1,2 *], Olivier Bertrand[1,2], Anne Caclin[1,2**], Jérémie Mattout[1,2**]

[1] Lyon Neuroscience Research Center, CRNL; INSERM, U1028; CNRS, UMR5292; Brain Dynamics and Cognition Team, Lyon, F-69000, France
[2] University Lyon 1, Lyon, F-69000, France

* Corresponding author
** Both authors equally contributed to this work.

Correspondence:
Françoise Lecaignard
INSERM U1028 - CNRS UMR5292
Centre de Recherche en Neurosciences de Lyon
Equipe DYCOG
Centre Hospitalier Le Vinatier (Bât. 452)
95, Boulevard Pinel
69500 Bron, France
francoise.lecaignard@inserm.fr

Telephone: 0033 472138963
Fax: 0033 472138901

Keywords: EEG and MEG source reconstruction
Data fusion
Bayesian model comparison
Group-level inference
Mismatch Negativity (MMN)
Early Deviance Response

Highlights

- Empirical evaluation of EEG-MEG source inversion is achieved in a Bayesian framework
- Multimodal information yields both a better fit and a reduced model complexity
- MEG was found more informative than EEG for auditory responses
- EEG proved useful to disambiguate between alternative spatial cortical models
- A highly precise spatio-temporal description of auditory generators was thus obtained

Abstract

We here turn the general and theoretical question of the complementarity of EEG and MEG for source reconstruction, into a practical empirical one. Precisely, we address the challenge of evaluating multimodal data fusion on real data. For this purpose, we build on the flexibility of Parametric Empirical Bayes, namely for EEG-MEG data fusion, group level inference and formal hypothesis testing.

The proposed approach follows a two-step procedure by first using unimodal or multimodal inference to derive a cortical solution at the group level; and second by using this solution as a prior model for single subject level inference based on either unimodal or multimodal data. Interestingly, for inference based on the same data (EEG, MEG or both), one can then formally compare, as alternative hypotheses, the relative plausibility of the two unimodal and the multimodal group priors. Using auditory data, we show that this approach enables to draw important conclusions, namely on (i) the superiority of multimodal inference, (ii) the greater spatial sensitivity of MEG compared to EEG, (iii) the ability of EEG data alone to source reconstruct temporal lobe activity; (iv) the usefulness of EEG to improve MEG based source reconstruction.

Importantly, we largely reproduce those findings over two different experimental conditions. We here focused on *Mismatch Negativity* (MMN) responses for which generators have been extensively investigated with little homogeneity in the reported results. Our multimodal inference at the group level revealed spatio-temporal activity

within the supratemporal plane with a precision which, to our knowledge, has never been achieved before with non-invasive recordings.

Introduction

Source reconstruction of electrophysiological responses have become a standard analysis in neuroimaging, as revealed by the increasing number of papers using such techniques, as well as the numerous methodologies afforded by electrophysiological analysis software. Whatever the methodology (Lecaignard and Mattout, 2015), the ill-posed nature of the underlying inverse problem remains (from a mathematical point of view, recognition of true generators is impossible). This issue calls for data carrying enough information about the underlying cortical generators, as it is more likely the case when bringing together EEG and MEG recordings as proposed more than 30 years ago (Cohen and Cuffin, 1987; Puce and Hämäläinen, 2017). This paper addresses the added value of combining EEG and MEG data for distributed source localization, which we evaluated here *empirically* with auditory mismatch responses.

Merging EEG and MEG aims at accounting for information missed by one modality and captured by the other one (Dale and Sereno, 1993; Fuchs et al., 1998), and crucially, at reducing the under-determined nature of the ill-posed inverse problem thanks to complementary information gathered by these two modalities (Plonsey and Heppner, 1967). Fused reconstruction therefore appears promising to reach high temporal and spatial resolutions in brain function imaging. Greater performances for fusion than separate EEG or MEG source reconstructions were indeed consistently reported in simulation-based studies. Quantitative evaluations rested on various metrics obtained from the comparison of the true distribution (that has generated the synthetic data) and reconstructed ones. In short, reduced localization errors could be reported for both superficial and deep sources (Fuchs et al., 1998), as well as for different signal-to-noise ratio (SNR) and sensor montages (Babiloni et al., 2004). Decrease of the undesirable sensitivity of inversion methods to source orientation (Baillet et al., 1999) was also reported. Further evaluation with empirical data is a necessary step, but in this case the lack of knowledge of the true cortical generators obviously prevents from using simulation-based metrics. To date, only few studies

attempted to circumvent this issue. Enhanced precision of source estimates was found with visual evoked responses (Henson et al., 2009). Other studies considered specific cases for which fMRI results (Sharon et al., 2007), widely described median nerve stimulation (Molins et al., 2008) or intracranial recordings with epileptic patients (Chowdhury et al., 2015) were assumed to provide the to-be-compared cortical source distribution. All these studies were in favor of reduced errors of localization with fused inversion.

In contrast to those approaches, a procedure for the multi-data integration was proposed by Henson and collaborators (2011) that enables the empirical assessment of multimodal inference. It followed a series of work, some of which we performed together, to demonstrate the flexibility and usefulness of Parametric Empirical Bayes (PEB) for solving the EEG or MEG inverse problem, incorporating several uninformed or informed (e.g. fMRI) priors, enabling the formal comparison of alternative prior models (Daunizeau et al., 2005; Friston et al., 2008b; 2006a; Henson et al., 2010; Mattout et al., 2005; 2006; Phillips et al., 2005), and for EEG and MEG simultaneous source reconstruction (Henson et al., 2009; 2011). This approach is the one implemented in the SPM software for EEG and MEG source reconstruction. In their approach, Henson and collaborators used the possibility to enforce (through strong priors) the precision (confidence) associated with each modality. Hence by accounting for both EEG and MEG data, or by switching off the influence of one or the other, they could empirically demonstrate the superiority of the fusion approach. Precisely, they report larger evidence for the fusion model (equal contribution of EEG and MEG), which translates into a larger accuracy (data fit) and a lower complexity (overfitting).

In the present study, we further exploits PEB and Bayesian Model Comparison (Penny et al., 2010) to illustrate a slightly different approach for the empirical assessment of the usefulness of EEG-MEG data fusion. We also extend the demonstration of such an empirical assessment to another dataset pertaining to two auditory oddball tasks. Our approach rests on model inversion for multiple subjects, that is constrained by a soft group spatial prior to guide individual source reconstruction. Importantly, beyond demonstrating the superiority of multimodal inference, it enables to address questions such as: “can EEG, MEG or fused data equally distinguish between close plausible inverse solutions?”. In other words, the

alternative approach illustrated here speaks to source model separability afforded by each modality. Interestingly, the obtained results provide some insights onto why the different modalities show different performance.

We applied the proposed evaluation scheme to auditory mismatch (or deviance) responses elicited by a change (or deviant) in a regular acoustic environment, including the well-known Mismatch Negativity (MMN) (Näätänen et al., 2007). This choice was motivated by the outstanding place the MMN has occupied in cognitive and clinical neuroscience (Auksztulewicz and Friston, 2016; Morlet and Fischer, 2014; Sussman and Shafer, 2014), contrasting with the arguably poor consistency of findings in the MMN source research (Fulham et al., 2014; Schönwiesner et al., 2007). Beside, recent findings of earlier mismatch responses than the MMN (Escera et al., 2014; Lecaignard et al., 2015) encourage to develop a comprehensive analysis of auditory responses to improve our understanding of auditory (deviance) processing. To date, only a few MEG studies addressed the localization of early deviance components (Recasens et al., 2014a; 2014b; Ruhnau et al., 2013), with activity circumscribed in the primary auditory cortex. Taken together, these recent findings indicate that it is time to combine high temporal and spatial information for an in-depth characterization of auditory deviance processing.

Strong efforts using different neuroimaging techniques have been made to identify the cortical generators of the MMN for about three decades. Functional Magnetic Resonance Imaging (fMRI) and electrophysiological techniques (EEG, MEG) were mostly employed, that favored spatial or temporal precision respectively. To our knowledge no study has been conducted using fused inversion (simultaneous recordings but separate source modeling were conducted in Huotilainen et al., 1998; Kuuluvainen et al., 2014; Rinne et al., 2000). Taken together, fMRI (see for review Deouell, 2007) and electrophysiological studies (Fulham et al., 2014; Giard et al., 1995; Lappe et al., 2013a; Marco-Pallarés et al., 2005; Recasens et al., 2014b; Ruhnau et al., 2013; Waberski et al., 2001) suggested that the most prominent sources are located in temporal and frontal areas. However, there is a large and acknowledged variability across findings (Deouell, 2007), obtained with various experimental designs (including different physical properties of stimuli), that prevents from a reliable and detailed description of the MMN network. It is possible that none

of these modalities may be sufficiently informed spatially and temporally when employed alone, which pleads for advanced methods such as fused reconstruction.

In this context, the aim of the current study was twofold: first, to propose a general method to evaluate finely and quantitatively the performance of multimodal and unimodal source reconstruction with empirical data. The second aim was to provide a detailed description of early and late auditory mismatch generators using advanced statistical methods including fused inversion (Henson et al., 2009). We considered data originating from a previous passive auditory oddball study (Lecaignard et al., 2015) with two deviance features (frequency and intensity, separately manipulated) and conducted with simultaneous EEG and MEG recordings. Our results demonstrate the larger source model separability of fused inversion and the great potential of such information integration that here produced a fine-grained description of a fronto-temporal network underlying auditory processing.

1. Material and Methods

We here briefly describe the source localization methodology employed in the present study including model inversion with group-level inference (Litvak and Friston, 2008) and EEG-MEG fusion (Henson et al., 2009). We then present our approach for the quantitative evaluation of EEG, MEG and fused EEG-MEG inversion, and the multimodal dataset used to validate our approach, resting on simultaneous EEG-MEG recordings of auditory frequency (FRQ) and intensity (INT) deviance responses.

1.1. Methods for source reconstruction

1.1.1. *Forward model computation.*

For both MEG and EEG modalities, a three-layer realistic Boundary Element Model (BEM) (Hämäläinen and Sarvas, 1989) was employed, with homogenous and isotropic conductivities within each layer set to 0.33, 0.0041 and 0.33 S/m for the scalp, skull and brain, respectively (Rush and Driscoll, 1968). The source domain included N_S=20484 sources (mean average distance = 3.4 mm) distributed on the

cortical mesh (grey-white matter interface) and we used surface normal constraints for dipole orientation. All meshes derived from canonical uniformly tessellated templates (provided with SPM8) that had been warped from individual MRI to account for subject-specific anatomy (Mattout et al., 2007). Coregistration of the resulting head model and functional data (EEG, MEG) was achieved for both modalities separately using each time a rigid spatial transformation based on three anatomical fiducials (nasion, left and right pre-auricular points) whose positions were measured relative to sensor ones for each modality (EEG: 3D digitization using a Fastrak Polhemus system, Colchester, VT, USA; MEG: monitoring head localization coils mounted on subject's head). For MEG data, head position was averaged across experimental sessions to allow for a common forward model between conditions. For each participant and each modality, computation of accurate BEM was performed with the software Openmeeg (http://openmeeg.github.io) (Gramfort et al., 2010). Re-referencing to the average mastoids was applied to EEG BEM. The resulting lead-field operator or gain-matrix $L \in \mathbb{R}^{N_c \times N_s}$ (with N_c sensors and N_s sources) embodying the pre-cited anatomical and biophysical assumptions, enters the following linear generative model M of data $Y \in \mathbb{R}^{N_c \times N_t}$(with N_t time samples):

$$Y = LJ + \varepsilon_n \quad (1)$$

where J represents the source distribution, i.e. the magnitude of dipole at each node of the cortical mesh, and ε_n represents the residual error term.

1.1.2. *Model inversion using Multiple Sparse Priors (MSP).*

Within a hierarchical Bayesian framework, we defined J as a multivariate Gaussian distribution of the form $J \sim \mathcal{N}(0, C_s)$ with $C_s \in \mathbb{R}^{N_s \times N_s}$ the (unknown) spatial source covariance. We assumed a multivariate Gaussian error term $\varepsilon_n \sim \mathcal{N}(0, C_n)$ with $C_n \in \mathbb{R}^{N_m \times N_m}$ the (unknown) spatial noise covariance (relatively to a normalized spatial space composed of N_m modes that will be defined in the following section). We used Multiple Sparse Priors (Friston et al., 2008b) to estimate both the distribution J that satisfies the general equation of linear model with Gaussian errors:

$$\tilde{J} = C_s L^t (C_n + L C_s L^t)^{-1} Y \quad (2)$$

and the posterior distribution of C_s and C_n. As described in Friston et al. (2008b), C_s is defined as a linear combination of N_p variance components $Q_s^i \in \mathbb{R}^{N_s \times N_s}$ corresponding to the sparse priors weighted by hyperparameters λ_s^i:

$$C_s = \sum_{i=1}^{N_p} \lambda_s^i \, Q_s^i \tag{3}$$

For the initial condition, we used SPM8 default sparse priors including 256 components in each hemisphere, and enabled inter-hemispherical coupling for each component leading to a total of $N_p = 712$ variance components. Estimation of the associated hyperparameters $\{\lambda_s^i\}_{i=1:N_p}$ was driven by the principle of source sparsity implemented in the Greedy-Search (GS) algorithm (Friston et al., 2008a). It should be noted that preliminary work (data not shown) using a various number of initial components did not reveal any significant change in the final outcome, which we attributed to the effectiveness of the sparsity constraint. At the sensor level, we assumed a single variance component equal to the identity matrix per modality and expressed in a normalized space (Henson et al., 2009) with hyperparameter weighting as follows:

$$\begin{cases} C_n = \lambda_e Q_e & for\ EEG\ inversion \\ C_n = \lambda_m Q_m & for\ MEG\ inversion \\ C_n = \lambda_e Q_e + \lambda_m Q_m & for\ fused\ inversion \end{cases} \tag{4}$$

In the case of fused inversion, matrices Q_e and Q_m are of same size (each having non-null modality-specific elements in separate part of the matrix to enable their concatenation in matrix C_n). MSP rests upon expectation maximization (EM) and provides Restricted Maximum Likelihood (ReML) estimates of hyperparameters $\lambda = \left\{\lambda_s^1, \ldots, \lambda_s^{N_p};\ \lambda_{modality}\right\}$, Maximum A Priori (MAP) estimate of J (Friston et al., 2007) and the free energy $\mathcal{F}$, an approximation of the posterior log-evidence of the model (the log-value of $p(Y|M)$, the probability of observing the data Y given the generative model M defined in Eq.(1); further details are provided in Appendix).

1.1.3. *Group-level inference*.

Group-level inference (Litvak and Friston, 2008) aims at specifying the prior distribution on the source covariance C_s by accounting for the assumption that distribution J should be common to all participants. This is a two-step procedure (Figure 1.A) that we used in the present reconstruction study (using SPM8) and that has also inspired our quantitative evaluation of fused inversion (see below):

- In the first step we perform a single *group-level* inversion using default sparse priors. Resulting posterior hyperparameters are thus informed by the group-level variance of the data; they provide a posterior on C_s (Eq.(3)).
- In the second step we proceed to *individual-level* inversions, starting with the group-informed posterior on C_s as prior, here referred to as *group priors*.

In practice, as detailed in Litvak and Friston (2008), the second step is left with two hyperparameters to estimate in the case of unimodal inversion ($\{\lambda_s;\ \lambda_e\}$ and $\{\lambda_s;\ \lambda_m\}$ for EEG and MEG inversions, respectively) and three terms in the case of fused inversion ($\{\lambda_s;\ \lambda_e, \lambda_m\}$). Prior to data inversion, group-level inference involves the normalization of the individual sensor-level data in a common spatial-mode space (Friston et al., 2008b). In short, this space is composed of N_m orthogonal virtual sensors (referred to as spatial modes) resulting from the singular value decomposition (SVD) of a group-informed gain matrix. Data reduction is also achieved using a subsequent projection of the data on temporal modes (Friston et al., 2006b). For each subject, the spatially and temporally projected data $\tilde{Y}_i \in \mathbb{R}^{N_m \times N_t}$ is rescaled (using the trace of $\tilde{Y}_i \tilde{Y}_i^t$) to accommodate signal amplitude differences over spatial modes. After model inversion, the reconstructed source activity J is projected on spatial modes and the percentage of data explained by J is computed to quantify the variance explained by J relative to the residual variance.

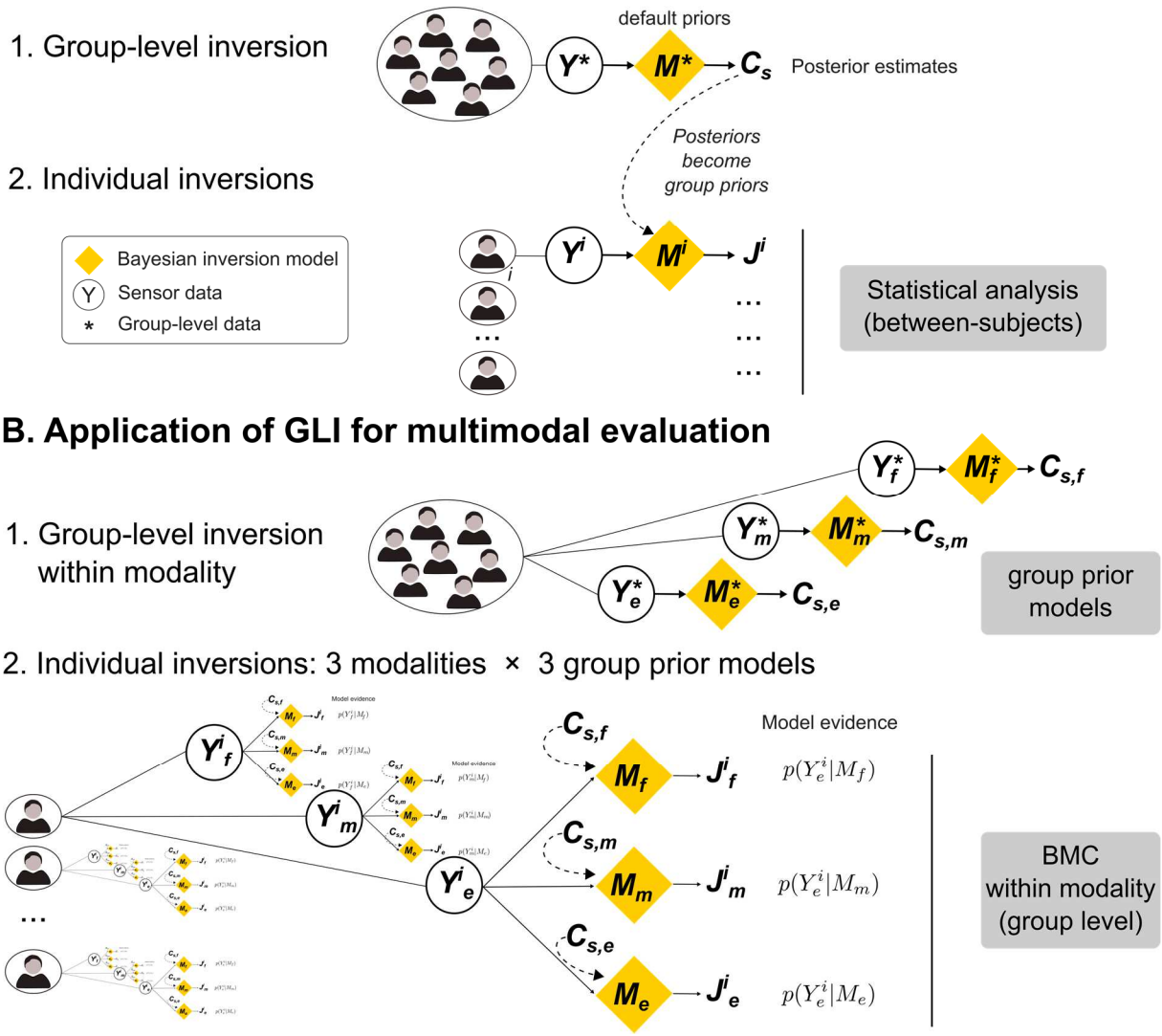

Figure 1. Procedure for multimodal evaluation. ***A. Schematic view of group-level inference*** *(Litvak and Friston, 2008). The two-stage procedure aims at constraining subject-specific inversion with empirical source priors reflecting cortical activity common to the group. Notations Y, M, C_s and J refer to sensor data, inversion model, source covariance and source distribution respectively, as specified in the main text. Mean distribution results from between-subjects statistical analysis.* ***B. Evaluation scheme.*** *The three separate group-level inversions performed for each modality provides the source priors for subsequent subject-specific inversions (nine per subject). After individual inversions, within each modality, Bayesian model comparison (BMC) proceeds at the group level using approximated model evidence to select which models (M_e, M_m or M_f) performs best. In this panel, model notation (M) is related to the modality of group priors only (subject superscript has been removed although inversion model is subject-specific) to highlight the fact that for each subject, the three competing models only differ with this respect.*

1.1.4. *Fused EEG-MEG inversion*.

The fused inversion approach proposed in Henson et al. (2009) was employed in the current study. This method entails the necessary rescaling of data and gain matrix over modalities to accommodate the different physical nature of signals. This rescaling leads to two crucial aspects: *(1)* projected data on MEG and EEG spatial modes become homogeneous and *(2)* sensor-level hyperparameters λ_e and $\lambda_m$can be quantitatively compared to assess the relative contribution of each modality to account for the variance of the observed data. Such comparison was conducted using paired Student's t-tests in the case of the MMN inversion ([150,200] ms) in condition FRQ and INT (see below).

1.2. Quantitative evaluation of separate and fused inversions

Bayesian Model Comparison (BMC) is a formal way to quantitatively compare models (M_1,M_2 ,...), based on their inferred model evidence ($p(Y|M_1), p(Y|M_2), \ldots$) that each quantifies how likely model M_i is to have generated data Y (Penny et al., 2010). In the present case, for each modality: EEG (e), MEG (m), and Fusion (f), we conducted a BMC that involved three models differing only on the group priors entering individual inversions. The three variants of group priors were inferred by the group-level inversion of EEG data (Y_e), MEG data (Y_m), and fused inversion of EEG and MEG data ($Y_f = [\tilde{Y}_e; \tilde{Y}_m]$) (Figure1.B, step1). These specific models entail the spatial information that could be captured by each modality over the group of subjects, and that we expect to vary across modality. In subsequent individual inversions (Figure1.B, step2), each group prior model will constrain the posterior estimate of source solution relatively to the spatial information conveyed by the inverted data. Our aim was to evaluate the ability of each modality to disentangle between the three resulting source distributions (BMC at the group level) and to compare such performances across modalities. Importantly, our approach is based on model separability whose relation to spatial resolution should be clarified. Spatial resolution usually refers to the finest elements that can be detected or characterized in a 2D or 3D image. However, in the context of EEG and MEG source reconstruction where cortical activity has to be inferred from scalp data by solving an ill-posed

inverse problem, a related but different and more important notion is the one of spatial discriminability or pattern separability. This refers to the ability of the data at hand to discriminate between two sets of cortical source distribution. Given the highly non-linear nature of the mapping between source locations and data topographies at the sensor level, distant sources on the cortical manifold may be harder to separate than closer ones. From now on, we use the terms spatial resolution, spatial discriminability or model separability interchangeably, to designate the ability of the given data, be it EEG, MEG or both, to discriminate between two inverse solutions in the sense of Bayesian model comparison.

To run the evaluation, a total of 9 inversions were computed for each subject: three modalities for data ($mod_d, with\ d \in \{e, m, f\}$) combined with three modalities for group priors ($mod_p, with\ p \in \{e, m, f\}$). For each data modality (mod_d), the three competing group prior models denoted M_e, M_m and M_f were confronted to the corresponding data (Y_{mod_d}), and resulting free energies approximating model evidence $p(Y_{mod_d}|M_e)$, $p(Y_{mod_d}|M_m)$ and $p(Y_{mod_d}|M_f)$ were thereafter compared across subjects with BMC using a random effect (RFX) model. This method provides the posterior exceedance probability of each model, which is the posterior belief that it is more likely than any others within the considered model space (Stephan et al., 2009). To further refine how group prior models manifest in inversion performance, we compare model accuracy (F_a) and model complexity (F_c) across models (for each quantity, 6 one-tailed paired Student's t-tests: models M_m *vs.* M_f in MEG and Fusion inversions, and models M_e *vs.* M_m in EEG inversion, in both FRQ and INT conditions). Finally, to account for inter-individual variability, we also computed the following free energy differences for each subject and for each modality mod_d, approximating the log-Bayes Factor:

$$\mathcal{F}_{mod_d, mod_{p=d}} - \mathcal{F}_{mod_d, mod_{p\neq d}} \approx \log\left(\frac{p\left(Y_{mod_d}\middle|M_{mod_{p=d}}\right)}{p\left(Y_{mod_d}\middle|M_{mod_{p\neq d}}\right)}\right) \quad (5)$$

Following the usual principles of Kass and Raftery (1995), a free energy difference (in absolute terms) lower than or equal to 3 indicates that models have comparable evidence: related group priors are of equal plausibility (inseparable models). Under

the assumption of non-identical group priors across modalities (EEG, MEG and fusion do not capture the same information), we would thus conclude that modality mod_d is not informed enough to discriminate between these different models. On the contrary, an absolute difference greater than 3 would support a large resolution of mod_d over model space. We expected *i)* EEG to have a poor capacity to separate group prior models, due to volume conduction which is acknowledged to degrade the spatial resolution of EEG (Vallaghé and Clerc, 2009) and *ii)* Fusion to have the largest model separability, being informed by the complementary EEG and MEG (Lopes da Silva, 2013). An original aspect of the proposed approach is that it allows a quantitative comparison of the EEG, MEG and Fusion source reconstructions applied to real data in a thorough way, by providing a detailed description of the inversion performance in each modality and by examining the individual variability in this performance. We carried out this empirical evaluation for the frequency and intensity MMN and early deviance response as described below.

1.3. Empirical data for source reconstruction and multimodal evaluation

Data originate from a passive auditory oddball study with simultaneous EEG-MEG recordings where the EEG analysis revealed two deviance responses: an early effect occurring within 70 ms after stimulus onset and a late effect (MMN) peaking at 170 ms post-stimulus (Lecaignard et al., 2015). We refer the reader to this study for a more detailed description of material and methods.

1.3.1. *Participants*.

27 adults (14 female, mean age 25±4 years, ranging from 18 to 35) participated in this experiment. All participants were free from neurological or psychiatric disorder, and reported normal hearing. All participants gave written informed consent and were paid for their participation. Ethical approval was obtained from the appropriate regional ethics committee on Human Research (CPP Sud-Est IV - 2010-A00301-38). Seven participants were excluded because they paid attention to sounds or their data was of low quality, leading the current analysis based on a total of 20 participants.

1.3.2. *Experimental design*.

Oddball sequences embedding either frequency or intensity deviants (conditions UF and UI in Lecaignard et al., 2015, here renamed as FRQ and INT, respectively) were considered in the present analysis. Both conditions involved the same deviant probability ($p = 0.17$). Two different frequencies (f_1=500 Hz and f_2=550 Hz) and two different intensities (i_1=50 dB SL (sensation level) and i_2=60 dB SL) were combined to define the four different stimuli that were used across conditions. Each condition (FRQ, INT) was delivered twice to enable reversing the role of the two sounds (standard and deviant). Further details about stimuli, sequences can be found in Lecaignard et al. (2015). Participants were instructed to ignore the sounds and watch a silent movie of their choice with subtitles.

1.3.3. *Data acquisition*.

Simultaneous MEG and EEG recordings were carried out in a magnetically shielded room with a whole-head 275-channel gradiometer (CTF-275 by VSM Medtech Inc.) and the CTF-supplied EEG recording system (63 electrodes), respectively. We provide here the aspects of particular relevance for the coregistration of multimodal data. Details regarding the simultaneous MEG and EEG recordings and the experimental setup can be found in (Lecaignard et al., 2015). EEG electrode positions relative to the fiducials were localized using a digitization stylus (Fastrak, Polhemus, Colchester, VT, USA) prior to the recordings. Head position relative to the MEG sensors was acquired continuously (sampling rate of 150 Hz) using head localization coils. Special care was taken to minimize head position drifts inside the MEG helmet between sessions. T1-weighted magnetic resonance imaging images (MRIs) of the head were obtained for each subject (Magnetom Sonata 1.5 T, Siemens, Erlangen, Germany). High MRI contrast markers were placed at fiducial locations to facilitate their pointing on MRIs and thereby minimize coregistration errors.

1.3.4. *Auditory event-related field/potential (ERF/ERP)*.

MEG evoked responses (2-45 Hz) were computed in exactly the same way as EEG ERPs (Lecaignard et al., 2015), with MEG-specific preprocessings, namely the rejection of data segments corresponding to head movements larger than 15 mm relative to the average position (over the 4 sessions) and to SQUID jumps.

Importantly, we only used time epochs that survived the procedures applied for artifact rejection for both modalities. EEG evoked responses were re-referenced to the average of the signal at mastoid electrodes in the current study for compatibility with the forward model. Grand-average responses at gradiometer MLP56 and electrode FCz in condition FRQ and INT are shown in Figure 2. Permutation tests (Lecaignard et al., 2015) revealed an early deviance and an MMN in both modalities (EEG, MEG) and both conditions.

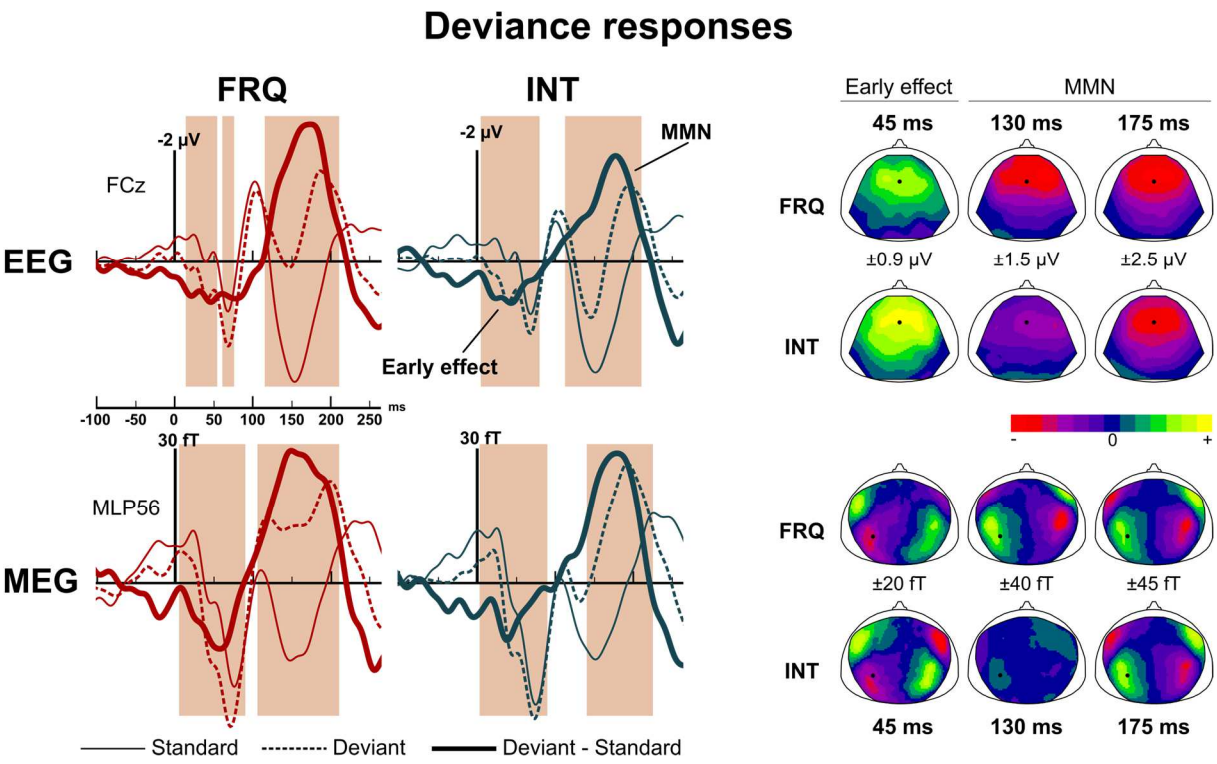

Figure 2. Mismatch ERPs/ERFs. *Left panel: auditory evoked responses at electrode FCz (upper row) and gradiometer MLP56 (lower row) for the frequency (left) and intensity (right) conditions. Shaded areas correspond to the time intervals of significant mismatch emergence over all sensors (modality-condition): (EEG-FRQ): [15 55] ms, [65 80] ms, [115 210] ms; (EEG-INT): [5 80] ms, [113 210] ms; (MEG-FRQ): [5 90] ms, [105 210] ms; (MEG-INT): [3 90] ms, [140 225] ms. Right panel: scalp topographies at relevant latencies for the early deviance, the rising edge and the peak of the MMN. Color-scale range is indicated for each map.*

1.3.5. *Data for source reconstruction.*

We used SPM8 software (Wellcome Department of Imaging Neuroscience, http://www.fil.ion.ucl.ac.uk/spm). Standard and deviant ERFs and ERPs (with averaged mastoid reference) were down-sampled (200Hz) for data reduction. Source reconstructions were estimated for difference responses (deviant-standard) in each

condition separately (FRQ, INT) and for each modality (EEG, MEG, Fusion). As sensor-level traces showed a tendency for the intensity MMN to start later than the frequency one, we distinguished the rising edge from the peak of this component to increase the spatial sensitivity of reconstructions. Three time windows were thus considered: from 15 to 75 ms (early deviance effect), from 110 to 150 ms (MMN rising edge), and from 150 to 200 ms (MMN peak). Importantly our comparative evaluation of separate (EEG, MEG) and fused (EEG-MEG) inversions was applied to the time interval [150,200] ms in both conditions (FRQ, INT). Regarding data normalization, 7 and 21 spatial modes (explaining 99.0% and 99.9% of the group-informed gain matrix variance) were retained for EEG and MEG, respectively. Data reduction using temporal modes was achieved for all inversions. The number of temporal modes allowing for 100.0% of the variance of the spatially projected data to be explained was equal to 6, 4 and 5 for [15, 75] ms, [110, 150] ms and [150,200] ms time intervals, respectively (for both modalities).

1.3.6. *Statistical analysis on source distributions.*

We conducted our statistical analyses at the group-level using the recent surface-based approach proposed in SPM12. Posterior estimates of source activity and associated variance at each node of the cortical mesh (the source domain) resulted from posteriors of $\tilde{J}$ and C_s. The energy of posterior mean was considered for statistical analysis. One-sample t-tests were performed at each node, thresholded at $p < 0.05$ with Family Wise Error (FWE) whole-brain correction. In addition, we imposed the size of subsequent significant clusters to be greater than 20 nodes. Distance between two local maxima within a cluster was constrained to be larger than 5 nodes.

2. Results

We first present the comparative evaluation for EEG, MEG and fused inversions that we conducted with FRQ and INT difference responses, at the MMN peak ([150, 200] ms). Second, as multimodal comparison was in favor of fused EEG-MEG inversion, we report the corresponding sources obtained for the time intervals [15, 75] ms, [110,

150] ms and [150,200] ms in the difference responses, in both conditions FRQ and INT, thus applying the current multimodal framework for source reconstruction to the localization of the sources of auditory mismatch responses.

2.1. Multimodal evaluation

Before presenting the results of our evaluation, we begin by controlling that source reconstruction of the MMN peak generators could be computed reliably (in terms of goodness of fit) for each modality and for each subject. This step also enables to point the similarities and differences in group-level results across modalities. We then provide a description of the different group priors obtained in each modality. Evaluation starts by the description of multimodal inversion performance to discriminate between group prior models, followed by a description of findings obtained in the two unimodal cases. These latter assess the respective sensitivity of each modality (EEG,MEG) which helps at better characterizing the outperformance of multimodal integration.

2.1.1. *Unimodal and fused MMN source distributions (qualitative comparison).*

The percentage of explained variance in condition FRQ was equal on average to 95.1% (± 2.1), 94.2% (± 2.3) and 93.6% (± 2.6) for EEG, MEG and fused inversions respectively. In condition INT, it was equal on average to 94.7% (± 2.5), 93.8% (± 2.3) and 93.1% (± 2.7) for EEG, MEG and fused inversions respectively. Regarding the contribution of each modality (EEG, MEG) in the case of fused inversion, paired Student's t-tests were used to compare the estimated values of hyperparameters λ_e and λ_m. In both condition FRQ and INT, inversions across subjects led to no significant difference between modalities (FRQ: group-average λ_e/λ_m : 0.018/0.041, t(19)=1.30, p=0.21; INT: group-average λ_e/λ_m : 0.022/0.051, t(19)=1.98, p=0.06).

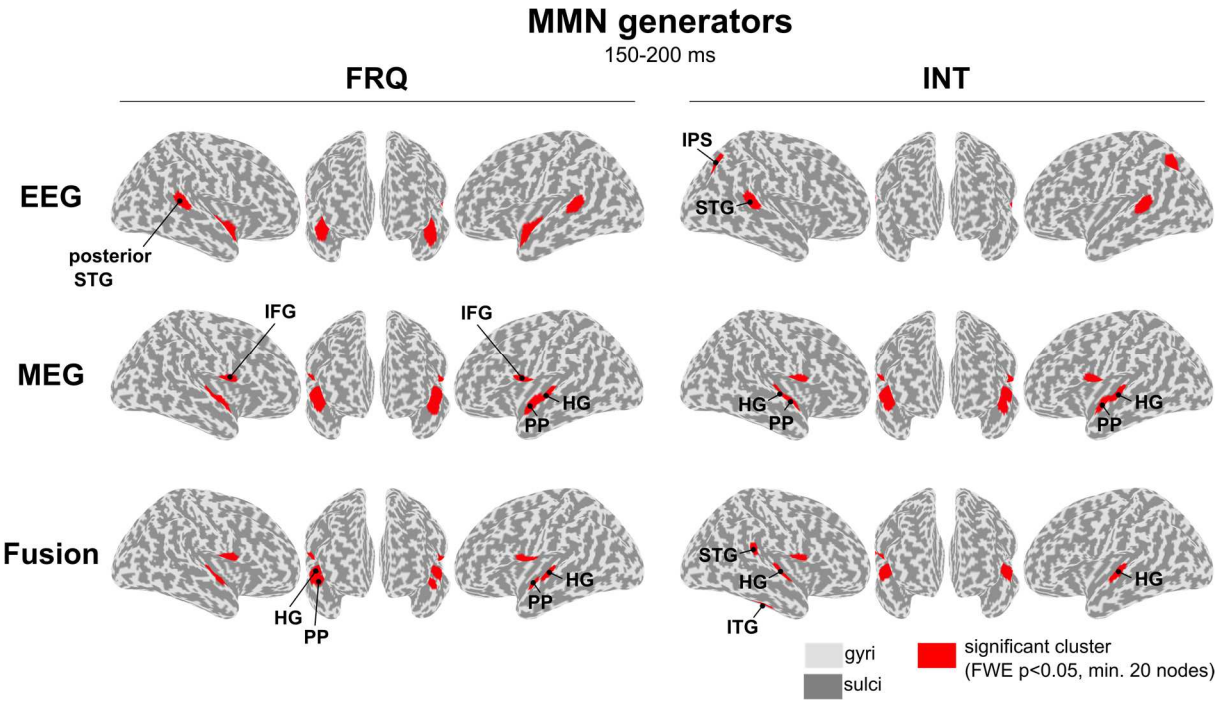

Figure 3. Mean source reconstructions of the MMN obtained in unimodal and multimodal inversions. *Left/Right panel: frequency/intensity MMN* ([150, 200] ms, *condition FRQ/INT). Red clusters indicate the significant source activity over the group (N=20) projected on the inflated cortical surface (HG=Heschl's gyrus; STG= superior temporal gyrus; P=planum polare; IFG=inferior frontal gyrus; IPS= inferior parietal sulcus; ITG=inferior temporal gyrus).*

Figure 3 shows the results of the statistical analysis projected on the inflated cortical surface in each modality (EEG, MEG and EEG-MEG) and each condition (FRQ, INT). In both conditions, EEG and MEG inversions led to different (but not inconsistent) reconstructed activity, and more focal clusters were found with fused inversion. Precisely,

- In condition FRQ, EEG inversion revealed bilateral activity in the anterior part of the supratemporal plane and in the lower bank of the posterior STG. No frontal area was found significant. MEG inversion indicated a large cluster in the supratemporal plane (number of nodes k > 120) expanding from the lateral part of HG through the Planum Polare (PP) in both hemispheres. A bilateral frontal area was located in the posterior IFG. The fused distribution comprised smaller supratemporal clusters (right: a single cluster (k=92) including the lateral part of HG and PP; left: separate clusters for HG (k=55) and PP (k=25)), and bilateral clusters similar to MEG ones in the frontal lobe.

- In condition INT, the EEG solution indicated bilateral activity in the posterior STG and the intraparietal sulcus (IPS). There was a similar distribution to condition FRQ with MEG. Fused inversion gave largest contributions in the lateral part of HG in both hemispheres, but also right clusters located in posterior IFG, posterior STG and in the inferior temporal gyrus (ITG).

In sum, this step validates the accuracy of the inversion scheme in each modality, suggests that EEG and MEG contributed equally to the fusion inversion, and finally reveals expected differences in EEG and MEG mean reconstructions that qualitatively motivates the fusion of these modalities to take benefit of their respective sensitivity.

2.1.2. *Group prior models* (Figure 4).

As expected, group priors varied across modalities while showing consistency across the main temporal clusters involved in auditory processing. EEG was found to upweight bilateral priors in posterior STG and the anterior temporal lobe in condition FRQ, and posterior STG, ITG and IPS in condition INT. In both conditions, MEG model upweighted bilaterally the supratemporal plane (lateral HG and PP) and posterior IFG. Fusion priors inferred from both EEG and MEG data involved similar cortical contributions to MEG (except the contribution of PP which was not present in condition INT) suggesting a larger informational value of MEG data. In both conditions and for all modalities, less restrictive priors (smaller cluster size and/or larger variance) were also found that we do not report here for they did not survive any individual inversion.

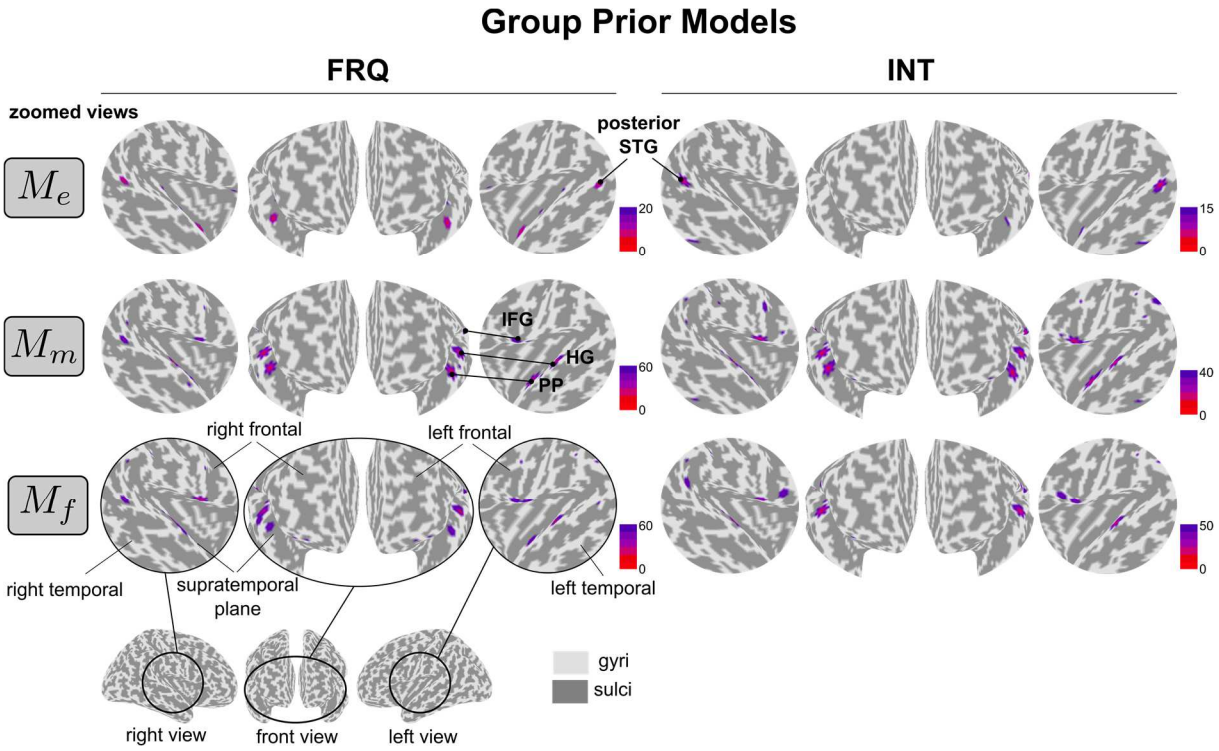

Figure 4. Group prior models for the evaluation scheme*. The three models were obtained in each modality (EEG, MEG and fusion inversions, separate rows) for the MMN peak* ([150, 200] ms)*. Left/Right panel: frequency/intensity MMN (condition FRQ/INT). For each modality and each condition, three zoomed views focusing on the supratemporal plane (with relation to the global view indicated at the bottom left) indicate the result of MSP inversion performed at the group level in the first step of group-level inference. Color scale for the variance of non-null (activated) nodes (arbitrary units) is mentioned for each model. Similarities of Fusion and MEG models suggest that MEG data is more informative than EEG about the spatial distribution of hidden neural generators of auditory responses.*

2.1.3. *Multimodal evaluation* (Figure 5).

We here describe the results obtained by manipulating the three group prior models ($\boldsymbol{M_e}$, $\boldsymbol{M_m}$ and $\boldsymbol{M_f}$) in the fused inversion. In both conditions, model $\boldsymbol{M_f}$ could be selected as the winning model at the group level (model exceedance probabilities given by BMC: $\boldsymbol{p(M_f|Y_f)}$=0.88 and $\boldsymbol{p(M_f|Y_f)}$=0.97 in FRQ and INT, respectively). This outperformance comes with both an improved model accuracy and a reduced model complexity relative to MEG model $\boldsymbol{M_m}$ (one-tailed paired Student's t-tests, $\boldsymbol{F_a}$: t > 2.69, p < 0.007 for both conditions; $\boldsymbol{F_c}$: t > 2.10, p < 0.025 for both conditions). Examination of within-subject variability reveals the robustness of model separability

across subjects. By setting the evidence threshold to 3, Fusion concludes in favor of model $\boldsymbol{M_f}$ over $\boldsymbol{M_e}$ in all subjects (both conditions), and in favor of model $\boldsymbol{M_f}$ over $\boldsymbol{M_m}$ in the majority of them (9 subjects out of the 12 that did give a conclusive result in FRQ, and 9/14 in INT). This suggests a reduced model separability between $\boldsymbol{M_f}$ and $\boldsymbol{M_m}$ compared to between $\boldsymbol{M_f}$ and $\boldsymbol{M_e}$, as illustrated in Figure 5, right-most graphs. To further characterize the separation between $\boldsymbol{M_f}$ and $\boldsymbol{M_m}$, we examined the putative gain or loss of model accuracy and model complexity when replacing original group priors ($\boldsymbol{M_f}$) by the ones from MEG ($\boldsymbol{M_m}$). Figure 7.A provides corresponding 2D graphs in the two conditions which clearly reveal the twofold loss (model accuracy and model complexity) obtained at the individual level with MEG priors. Figure 7.A also shows the minority of subjects for whom model $\boldsymbol{M_m}$ was winning over $\boldsymbol{M_f}$ (represented by red dots on the graphs; 3 and 5 subjects in conditions FRQ and INT, respectively). In these singular cases, the same pattern could be observed, namely complexity between models was found nearly equal while the MEG priors systematically yielded a better fit. This suggests that model $\boldsymbol{M_f}$ corresponds to a local minimum for these particular subjects, and illustrates that empirical (group) priors constitute soft constraints on individual solution that can be ruled out when confronted to divergent informative data.

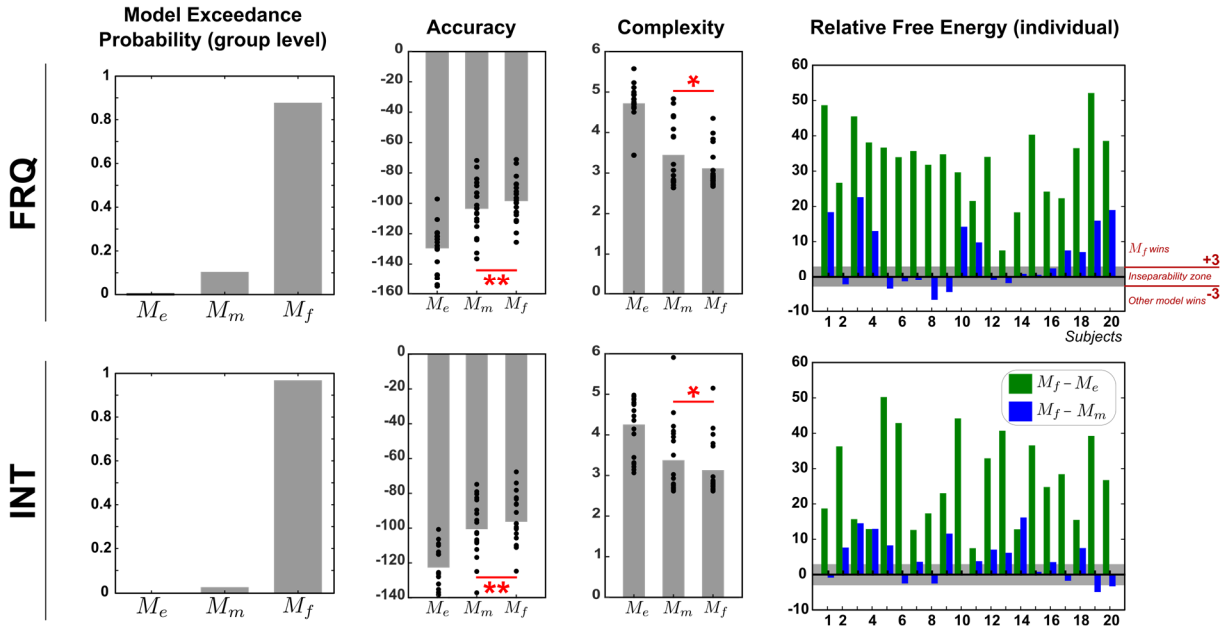

Figure 5. Model comparison based on fused EEG-MEG data. Group prior model comparison in the fused inversion, for each condition (top row: FRQ, frequency deviance; Bottom row: INT, intensity deviance). On each row, left-most graph: Bayesian model comparison (BMC) of group prior models ($\boldsymbol{M_e}$, $\boldsymbol{M_m}$and $\boldsymbol{M_f}$). Fused priors ($\boldsymbol{M_f}$) have by far the largest model exceedance probability in both conditions. Middle graphs: model accuracy and model complexity (the two parts of the free-energy, see main text for details):bar and dot plots represent the mean and individual values for each model, respectively. Red stars illustrate the results from the one-tailed paired Student's t-tests (:p<0.05; **:p<0.01). Right-most graph: the difference in free energy relative to Fusion model for all subjects is plotted as a bar chart (green: EEG model; blue: MEG model). Grey area indicates the zone where models are not separable under an evidence threshold of 3.*

2.1.4. *Unimodal evaluations*.

Regarding the EEG inversion (Figure 6.A), BMC clearly decided in favor of model $\boldsymbol{M_e}$ with model exceedance probabilities $\boldsymbol{p(M_e|Y_e)} = 1$ in both conditions. This result leverages on an increase of model accuracy only ($\boldsymbol{M_e}$ vs. $\boldsymbol{M_m}$ in both conditions, $\boldsymbol{F_a}$ one-tailed t > 6.44, p < 0.001; $\boldsymbol{F_c}$ one-tailed t < -2.35, p > 0.98). However, examination of individual free energy differences puts the group-level performance into perspective and rather suggests a poor ability of EEG to separate models. Precisely, although model $\boldsymbol{M_e}$ could always provide the largest free energy (except in

2 subjects with MEG group priors and 1 subject with Fusion priors in condition INT), low amplitudes of free energy difference prevented from disentangling models. Under the evidence threshold of 3, models $\boldsymbol{M_e}$ and $\boldsymbol{M_m}$ were not separable in the majority of subjects in both conditions (18/20, 15/20 in FRQ and INT, respectively), and similar findings were obtained with $\boldsymbol{M_e}$ and $\boldsymbol{M_f}$ (13/20, 19/20 in FRQ and INT, respectively).

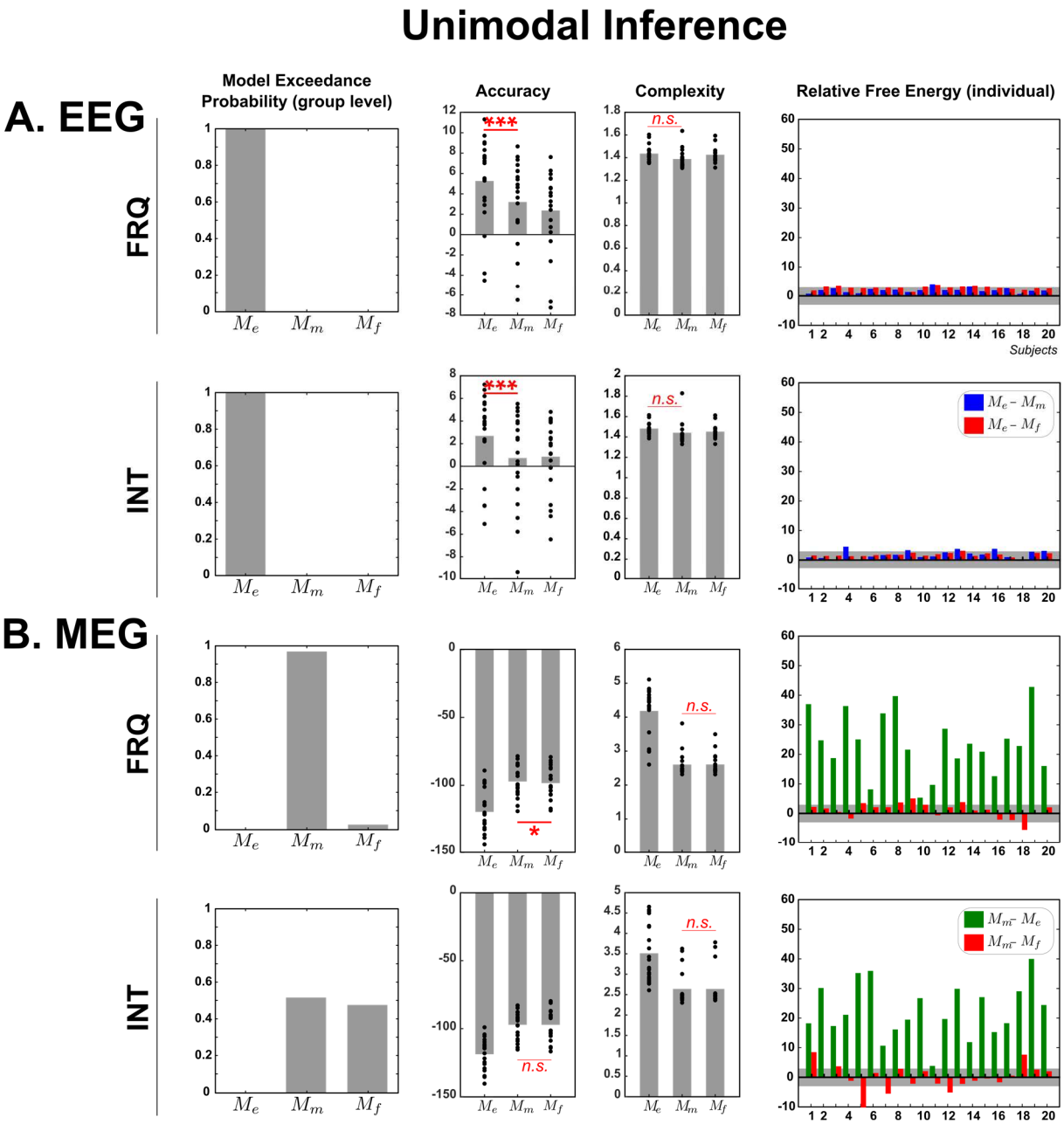

Figure 6. Model comparison based on EEG and MEG data, separately. *Group prior model comparison in the EEG (panel A) and the MEG (panel B) inversions. Results are presented using the same framework as for the multimodal evaluation (Figure 5). Middle graphs: statistical analysis is indicated (red) whenever it was conducted (n.s.: non-significant, p≥0.05; *:p<0.05; **:p<0.01). Right-most graphs:*

legend captions in condition INT plots indicate the color code used for the modalities concerned in the free energy differences.

Regarding the MEG inversion (Figure 6.B), group-level BMC could separate $\boldsymbol{M_e}$ from $\boldsymbol{M_m}$ in favor of the later model in both conditions. This finding emerges strongly from the large free energy differences observed in all subjects (Figure 6.B right-most graphs). In contrast, separability of MEG and Fusion priors ($\boldsymbol{M_m}$ vs. $\boldsymbol{M_f}$) appears less clearly and differs across conditions. In condition FRQ, BMC selected MEG priors ($\boldsymbol{p}(\boldsymbol{M_m}|\boldsymbol{Y_m})$=0.97) which manifest with a larger model accuracy (one-tailed t = 2.08, p = 0.026) but no significant difference in model complexity (one-tailed t = 0.07, p = 0.473). Individual inspection shows that MEG inversion led to inconclusiveness in the majority of subjects (14/20) but could select model $\boldsymbol{M_m}$ over $\boldsymbol{M_f}$ in 5 out of the 6 remaining subjects. In condition INT, inseparability of models $\boldsymbol{M_m}$ and $\boldsymbol{M_f}$ was found at the group level ($\boldsymbol{p}(\boldsymbol{M_m}|\boldsymbol{Y_m})$ =0.52 and $\boldsymbol{p}(\boldsymbol{M_f}|\boldsymbol{Y_m})$ =0.48) and was confirmed by the absence of difference between model accuracy or model complexity (one-tailed t < 0.03, p > 0.487). Such inseparability was dominant in the group (14/20 subjects) and contrary to condition FRQ, model $\boldsymbol{M_m}$ was not clearly preferred among the 6 other subjects (3/6 preferred $\boldsymbol{M_m}$, 3/6 preferred $\boldsymbol{M_f}$). To further address this difference between conditions, that was not present in the fused inversion, we examined the effect of group prior change (from $\boldsymbol{M_m}$ to $\boldsymbol{M_f}$) in model accuracy and model complexity. Results are shown in Figure 7.B, which discloses a larger within-subject variability in model accuracy in condition INT (number of subjects with improved/reduced accuracy: 10/10 in condition INT; 15/5 in condition FRQ).

Finally, an important observation is that in the unimodal inversions, fused priors led predominantly to inseparability when compared to the original group priors (M_e in the EEG inversion, M_m in the MEG inversion) namely 13/20 and 19/20 subjects in the EEG inversion, in condition FRQ and INT, respectively, and 14/20 subjects in the MEG inversion (both conditions).

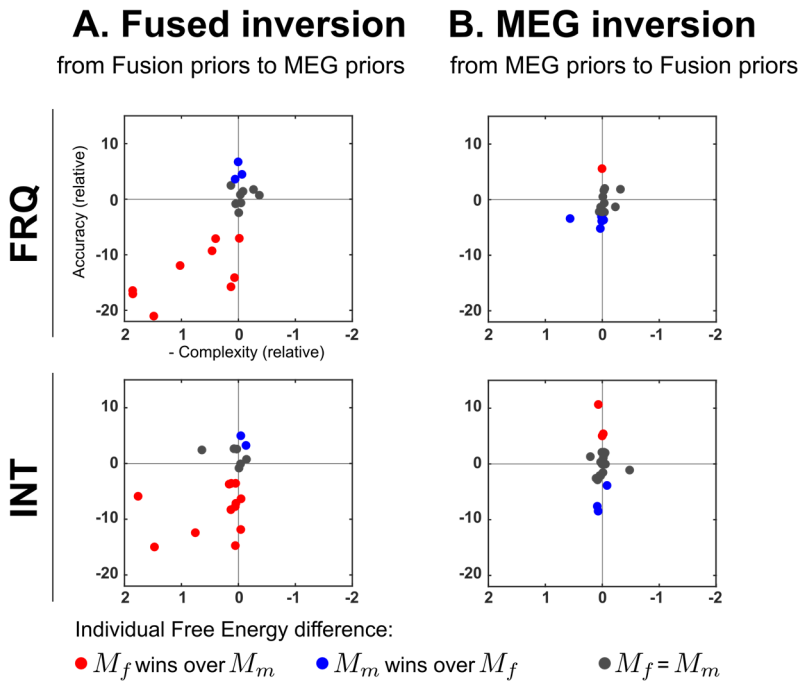

Figure 7. Separability of Fusion and MEG group prior models. A. In the fused inversion. *For each condition, (top/bottom: FRQ/INT) dots represent for all subjects the change in model complexity as a function of change in model accuracy when switching from Fusion model (the original priors in the fused inversion scheme) to MEG model. For a better understanding, the complexity axis has been reversed, so that the top-left corner of the plot hosts subjects showing a performance improvement (model change induces larger accuracy, lower complexity) whereas the bottom-left corner is related to individual degradation. In addition, dots are sorted according to model separability based on the relative free energy difference (bar charts in Figures 5 and 6.B) under an evidence threshold of 3. Color code is indicated in the legend. In both conditions, the majority of subjects show reduced performance with MEG model, leveraging on both accuracy and complexity terms. B.* ***In the MEG inversion.*** *The plots here indicate the changes when replacing the original MEG priors by the Fusion model. Here, these 2D representations reveal the lack of effect on complexity in both conditions, and the larger inhomogeneity of the group in the INT condition, as the group splits into two parts of equal size along the accuracy dimension.*

2.1.5. *Summary.*

Our evaluation approach relying on group prior model comparison succeeded at quantifying the performance of each modality for the reconstruction of empirical data. We found a large and robust model separability in the multimodal inversion, where the integration of EEG and MEG data enabled to enhance model accuracy and reduce model complexity. Such performance could not be achieved with unimodal inversions. Precisely, EEG exhibited a poor ability to discriminate between the three models, as evidenced by the majority of individual indeterminations encountered in

both conditions. The MEG inversion proved to be similar to the Fusion scheme for separating and selecting original priors against EEG ones, but revealed limited performances with Fusion priors, an effect that was further found sensitive to inter-individual variability. The twofold better performance of MEG over EEG (more plausible spatial priors with unimodal and multimodal inferences, and larger spatial discriminability) speaks to the fact that MEG was found here more informative than EEG. Moreover, and interestingly, its failure to reach the multimodal performance also ascertains its complementarity with EEG. In the following section, we present the deviance-related source reconstructions inferred from multimodal data, here evidenced as the most informative modality.

2.2. Fused EEG-MEG sources for auditory mismatch responses

w

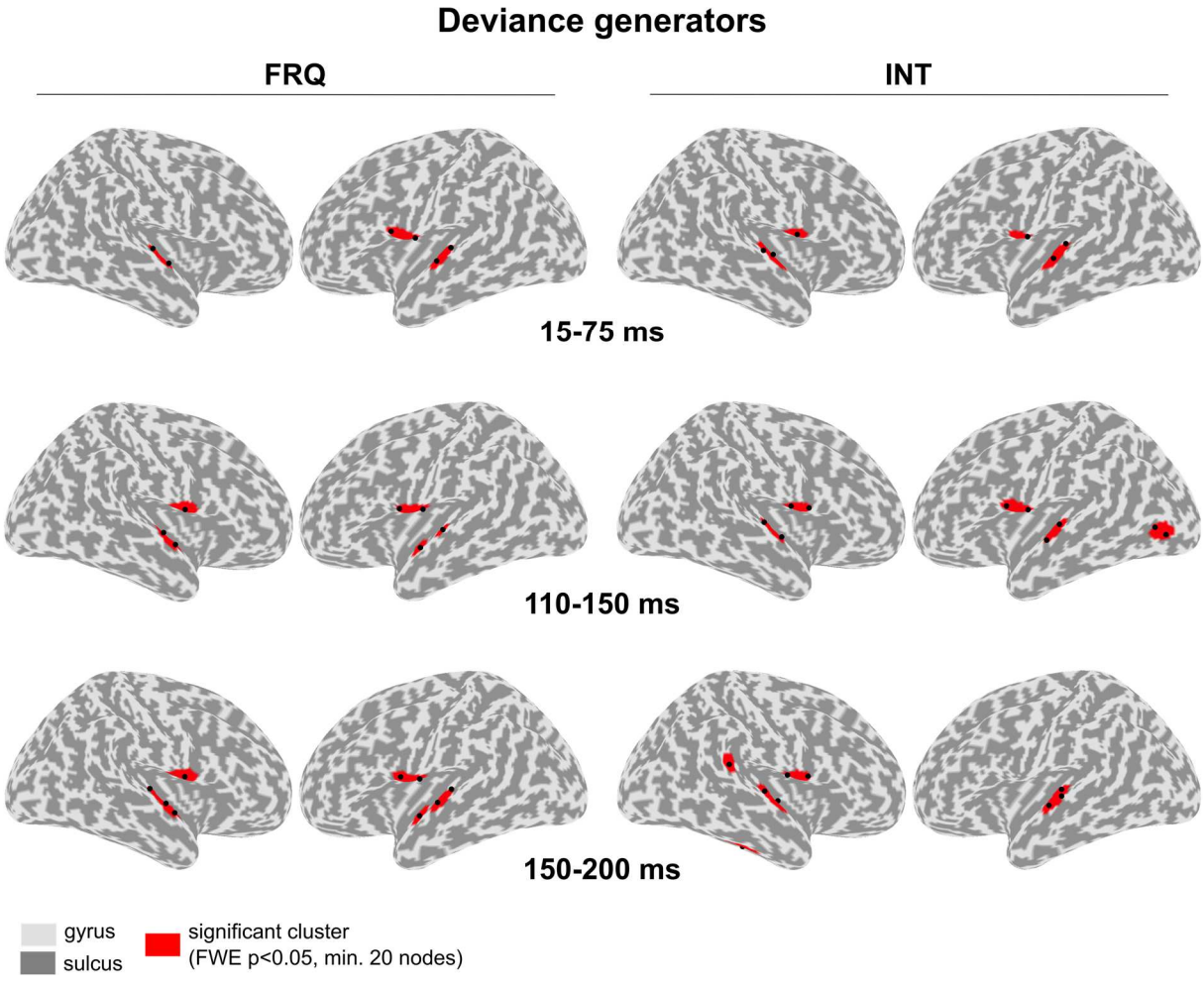

Figure 8. Deviance generators (fused MSP reconstruction). *Significant clusters (red) are displayed on the inflated cortical surface (right and left views) for each time interval (rows) and each condition (frequency=left panel, intensity=right panel). Black dots indicate the local maxima within each cluster (with a minimum distance of 5 adjacent nodes). MNI coordinates are provided in Table 1 (frequency) and Table 2 (intensity).*

Figure 8 shows the results obtained for each deviance type and each time interval with fused inversion. Cluster sizes and peak location in MNI space for each local maxima for significant activated areas are summarized in Table 1 for condition FRQ, and Table 2 for condition INT.

2.2.1. *Condition FRQ.*

Reconstructions of deviance generators within time windows [15, 75] ms, [110, 150] ms and [150,200] ms were performed with the percentage of explained variance equal on average to 90.7% (± 4.8), 92.3% (± 4.4) and 93.6% (± 2.6), respectively. Early-deviance effect ([15, 75] ms) was found to involve HG in both hemispheres and left posterior IFG. Following this, reconstruction of the rising edge of the MMN ([110, 150] ms) indicated supratemporal activity in HG and PP, within a large cluster in the right hemisphere (comprising two local maxima), and separated in two distinct clusters in the left hemisphere (with HG cluster being smaller). Significant activity was also found in bilateral posterior IFG. Finally, as described in previous section, the peak of the MMN ([150,200] ms) was associated with activity in both hemispheres peaking in HG, PP and posterior frontal IFG. The total number of significant nodes within bilateral supratemporal planes was larger for the peak than for the rising edge of the MMN (178 and 108 respectively), while it remained constant within IFG (116 and 112 respectively).

FRQ	Side	Source Cluster	Cluster Size	Peak Location		
Early deviance, [15 75] ms	L	HG	56	-60	-9	2
				-45	-23	7
	R	HG	57	59	-3	2
				48	-17	6
	L	IFG	50	-53	10	15
				-58	-2	2

MMN Rising Edge, [110 150] ms	L	HG	19	-54	-12	4
	L	PP	21	-49	-8	-10
	R	HG/PP	68	52	-8	4
				49	-7	-8
	L	IFG	57	-56	6	9
				-56	-6	8
	R	IFG	55	57	2	6
MMN Peak, [150 200] ms	L	HG	55	-60	-9	2
				-45	-23	7
	L	PP	25	-50	-6	-8
	R	HG/PP	92	55	-5	4
				48	-19	6
				49	-7	-8
	L	IFG	55	-56	6	9
				-53	-6	6
	R	IFG	61	57	2	6

Table 1. Results of MSP inversion for frequency deviance with fused inversion. Cluster Size: number of cortical mesh nodes. Peak Location: MNI coordinates in mm.

2.2.2. *Condition INT.*

The percentage of explained variance was equal on average to 91.4% (± 5.2), 90.5% (±5.4) and 93.1% (± 2.7) for the reconstructions within time windows [15, 75] ms, [110, 150] ms and [150,200] ms, respectively. Within the early-deviance window ([15, 75] ms), activity was mostly found in bilateral HG but was also located in posterior IFG. Reconstructions within [110, 150] ms produced significant clusters in bilateral HG and posterior IFG. In addition, there was a spurious contribution from left middle occipital gyrus (MOG). Finally, sources in HG and posterior IFG were observed in both hemispheres for the MMN peak reconstruction ([150,200] ms). Smaller clusters were found in ITG and posterior STG in the right hemisphere. With the thresholds chosen in the current study, no contribution of PP could be reported at any latency.

INT	Side	Source Cluster	Cluster Size	Peak Location		
Early deviance, [15 75] ms	L	HG	70	-58	-10	5
				-43	-25	9
	R	HG	71	49	-11	4
				55	-16	3
	L	IFG	28	-58	-2	2
	R	IFG	37	57	2	6

MMN Rising Edge, [110 150] ms	L	HG	55	-48	-18	5
				-59	-11	-5
	R	HG	56	59	-3	2
				48	-17	6
	L	IFG	57	-55	8	13
				-58	-2	2
	R	IFG	45	51	9	5
				57	0	12
	L	MOG	46	-41	-74	-1
				-40	-74	4
MMN Peak, [150 200] ms	L	HG	76	-45	-20	6
				-61	-9	-2
				-60	-18	2
	R	HG	77	49	-16	3
				50	-9	0
	R	STG	33	62	-37	20
	R	ITG	31	57	-29	-27
	R	IFG	46	51	6	5
				51	-3	14

Table 2. Results of MSP inversion for intensity deviance with fused inversion. Cluster Size: number of cortical mesh nodes. Peak Location: MNI coordinates in mm.

2.2.3. *Summary*.

The fused reconstructions of deviance responses observed in ERP/ERF revealed a bilateral fronto-temporal network in both conditions (FRQ, INT). Temporal activity was clustered in the supratemporal plane, where fused inversion improved the spatio-temporal description of deviance-related activity. In particular, fused inversion could separate HG and PP clusters spatially, but also temporally as PP contribution varies over time and across conditions. Frontal contributions could be recovered in both conditions as soon as the early deviance window.

3. Discussion

In the present study, we proposed an original and generic approach to address the long-standing question of the benefit of EEG-MEG data fusion to infer cortical activity. This approach rests on hierarchical empirical Bayesian modelling and Bayesian model comparison to disentangle between alternative spatial models using empirical data. This departs from most former fusion approaches that could only be formally evaluated using simulated data. Furthermore, in contrast with previous Bayesian approach (Henson et al., 2011), we conduct this assessment in the context of group level inference, which enables the formal comparison of spatial priors derived from unimodal and multimodal group data at the individual level. To our knowledge, the method used here is also the first to combine: realistic forward modelling, hierarchical empirical Bayesian inference, group-level and fused EEG-MEG inference, and surface-based statistics. Finally, we applied this framework to the important issue of localizing the sources of the auditory MMN, a component that is very much studied and used as a marker of perceptual processes and their alterations in various neurological and psychiatric conditions (Carbajal and Malmierca, 2018; Friston, 2005; Näätänen et al., 2012).

Our results conclude in favor of the superiority of data fusion for source reconstruction in this context. Importantly, model comparisons at the group level and then at the individual level also shed light on the specific characteristics of each modality and on the complementarity of the EEG and MEG. This aspect is rarely examined with real data, in a quantitative manner. Fused inversion applied to early and late deviance responses resulted in a fronto-temporal network consistent with existing findings obtained from EEG or MEG alone, but described here, to our knowledge, with an unprecedented spatio-temporal finesse.

A formal approach to compare unimodal and multimodal inference for source reconstruction.

Our approach offers an alternative to the one proposed by Henson et al. (2011) which also relied on the Bayesian framework to evaluate the benefit of EEG and MEG data fusion. As noted by the authors, "*Because the model evidence is conditional on the data, one cannot evaluate the advantage of fusing MEG and EEG simply by comparing the model evidence for the fused model relative to that for a*

model of the MEG or the EEG data alone". They circumvented this obstacle by comparing three alternative models for the multimodal inference, varying the measurement noise prior of EEG and MEG to simulate unimodal EEG data (MEG data is only noise), MEG data (EEG is only noise) and multimodal data (EEG and MEG are both informative). A formal model comparison concluded that fusion is the most informative approach and that MEG is more informative than EEG.

In contrast we adopted a two-step approach that we applied for unimodal and multimodal inference. First, using a fixed effect analysis, we derived the most likely subset of sources at the group level, given each unimodal data or multimodal data. This led to three alternative models which we could then compare formally, at the individual level, based either on fused EEG and MEG data, or EEG and MEG data taken separately. This is interesting because it enables to assess, for each modality independently, how much this modality is able to distinguish between different but plausible sets of source locations. And given that these prior sets of locations reflect the sensitivity of each modality, this enables to compare EEG, MEG and fusion in their ability to reproductively select spatial models derived from the same data type over subjects, or on the contrary, to show poor specificity by expressing no preference.

Of course, it should be borne in mind that, as in the work by Henson et al. (2011), our framework for model comparison rests on the Variational Bayes (VB) approximation to the model log-evidence (the free energy) which could potentially impact the outcome of model selection. This issue was precisely addressed in Friston et al. (2007), using synthetic EEG data, in a context very similar to ours (hierarchical linear generative models). Not only BMC was found to recognize the true generative model of the simulated data among alternative candidates, but VB log-evidence approximations for all models were found very close to the ones obtained with MCMC, a sampling method assumed to provide an exact inference (but see also Litvak et al., 2019 in the case of hierarchical non-linear dynamic models). These previous findings demonstrated the face validity of VB for BMC in this context. Furthermore, our comparison between modalities was here further supported by the separate report and assessment of model Accuracy and Complexity. These analyses were in line with the outcome of BMC based on the free energy and afforded a further refined description of the relative specificity of EEG, MEG and data fusion.

The present procedure proves to be very rich in lessons, as modalities could be compared in terms of both the spatial priors they provide, and the spatial discriminability they enable. This is nicely illustrated by our findings with EEG and MEG taken alone. Indeed, EEG and MEG estimated different contributions from temporal and frontal sources, hence reflecting their different spatial sensitivity. However the source distribution inferred with EEG was mostly rejected by the MEG data as a poor model, but not the other way round.

Overall, this approach, here applied to auditory data, led to several important findings: notably the weak spatial discrimination power of the EEG; the higher sensitivity of MEG to inter-subject variability, which goes along with a higher spatial discrimination power; the robustness of multimodal inference which compensates for these limitations of unimodal inference (see below for further discussion).

About the difference and complementarity of EEG and MEG recordings.

The empirical evaluation we performed in two separate conditions, for reproducibility, shows that the inference based on multimodal data was able to finely discriminate between alternative plausible spatial priors, and to select the most informed one (the group prior derived from combined EEG and MEG data), in most subjects. Precisely, the higher free energy afforded by the multimodal priors was driven by both a higher accuracy and a reduced complexity.

This contrasts with what we observed with the unimodal based inferences, where model complexity was not improved by considering the group prior from the same modality. This is important because, taken together, these results promote multimodal integration not only because it provides a higher goodness of fit, as traditionally observed with simulation-based studies, but also because it offers a generalizable solution over subjects. In other words, multimodal inference yielded a highly plausible solution common to all subjects, which also provides optimal priors at the individual level to accommodate the between-subject variability.

As a validity check, we controlled that the two modalities were indeed afforded similar weighting by the empirical multimodal Bayes inference. In agreement with Henson et al. (2011) findings, we found no significant difference between precision noise

parameters at the sensor level[1]. This confirms that the superiority of multimodal inference is indeed due to a combination of EEG and MEG recordings.

Of course, this is to be concluded in the context of auditory mismatch responses. However, it is likely to be generalizable to any brain regions whose activity can be at least partly captured by both EEG and MEG sensors.

Our evaluations of unimodal inferences helped further characterizing the complementarity between EEG and MEG which are assumed to capture different aspects of the same underlying biophysical phenomena (Lopes da Silva, 2013). An illustration was given here where, at the scalp level, a difference in topographies between the frequency and intensity MMN could only be clearly observed with MEG. It is well known that EEG and MEG are not sensitive to the same source locations and orientations, as well as to the same biophysical properties of the head tissues (Lecaignard and Mattout, 2015). This certainly explains the differences in performance and source distributions here obtained with EEG and MEG based inference, respectively (Figure 3). Remarkably, our procedure allows to reveal and operationalize those differences.

Precisely, EEG proved able to extract relevant group-level priors that could best constrain individual inversions (model M_e obtained a very high exceedance probability at the group level when using EEG data alone). This clearly ascertains that EEG can be used reliably for source reconstruction studies, at least in the auditory domain. However, individual inspection reveals a rather weak ability to distinguish between spatial models across an homogeneous group of subjects (superiority of model M_e is a non-significant effect but present in all subjects). The MEG and Fusion models provided different group-informed cortical solutions (as can be seen notably in the supratemporal regions, Figure 4) but they turned out to be plausible alternative candidates in the eyes of EEG. This clearly resonates with the expected poorer spatial resolution with EEG (Puce and Hämäläinen, 2017).

This work also provides new perspectives on the information conveyed by MEG signals. The MEG model qualitatively exhibited more similarities with the Fusion

[1] Note that this finding was obtained under the commonly used assumption of independent and identically-distributed sensor noise. This assumption yields limited effect on data scaling performed during the inversion as suggested in Henson et al. (2009) with MEG.

model than with the EEG one (Figure 4). This suggests that fusion priors were primarily informed by MEG data, which, in a Bayesian setting, should be related to greater reliability. Furthermore, in multimodal inference, the MEG model was not selected but showed a smaller separability with the winning Fusion model than the EEG model (this is clearly visible on the individual bar charts in Figure 5, which enables to compare the evidence in favor of each model). Hence MEG appears as significantly more informative than EEG, in the present case of auditory data. This is again in full agreement with the expected higher spatial resolution with MEG than EEG (Babiloni et al., 2009) , and in particular within the temporal lobe (Poeppel and Hickok, 2015).

However, MEG data alone in condition INT, failed to separate the MEG and Fusion models. This results may be attributable to the group heterogeneity, which was not observed in the other two modalities. This speaks again for a higher spatial sensitivity of MEG recordings, whose consequence here would be that precise group-informed solutions become likely to be less accepted at the individual level in the few subjects who most deviate from the group (conversely, the EEG suffering from greater spatial blurring would be less sensitive to between-subject variability). Most importantly, the integration of EEG with MEG data (Fusion model, and multimodal inversion) enables to resolve this issue.

About the generators of Mismatch responses.

The comparative analysis performed at the peak of the MMN strongly encouraged us to merge EEG and MEG data to finely characterize the sources of other mismatch responses, as never done before. The main finding of this subsequent analysis is the identification of a bilateral fronto-temporal network at play during early and late deviance responses, for both conditions (FRQ, INT). The MMN findings (including the rising edge and the peak of the MMN) is totally consistent with the existing literature supporting fronto-temporal generators (Andreou et al., 2015; Auksztulewicz and Friston, 2015; Fulham et al., 2014; Lappe et al., 2013b; Marco-Pallarés et al., 2005; Recasens et al., 2014b; 2015; Rinne et al., 2000; Schairer et al., 2001). Perhaps the most striking point in comparison with these EEG or MEG studies is that expected contributions (frontal and temporal, bilateral) could be all identified at once and with a far larger spatial specificity (in the supra-temporal plane in particular) than usually observed. The present findings rather resemble those obtained with fMRI, as

reported by Schönwiesner and collaborators (2007). From a qualitative point of view, fused inversion could thus reach the spatial resolution of fMRI (at least in the temporal lobe), which made possible to reveal distinct spatial patterns across specific time intervals in the first 200 ms of auditory processing (which is obviously not feasible with BOLD signals). In particular, we could observe a posterior to anterior progression in the supratemporal plane (from HG to PP), between the rising edge and the MMN peak for the frequency condition, in line with several studies that explored the N1 and MMN generators (Recasens et al., 2014a; Scherg et al., 1989). Note also, that the comparison of the frequency and intensity conditions shows subtle spatio-temporal patterns: similar activations at early latency are followed by differences within the supratemporal plane and frontal regions during the MMN. This supports different sensory processes at the MMN latency, as proposed by early ECD studies conducted with EEG (Giard et al., 1995) and MEG (Levänen et al., 1996). Regarding early deviance generators, temporal activity was clearly circumscribed within bilateral Heschl's gyrus for both deviance features. This is totally consistent with MLR findings from intracranial recording studies (Liégeois-Chauvel et al., 1994; Pantev et al., 1995; Yvert et al., 2002). Recent MEG studies also reported temporal contributions including from HG, in the right hemisphere (Recasens et al., 2014a) and bilaterally (Recasens et al., 2014b). Crucially, a major difference with these studies pertains to frontal sources that we were able to recover. Under the assumption of a hierarchical anatomo-functional organization for deviance processing, which would cover subcortical areas up to associative cortical regions (Escera and Malmierca, 2014), such early frontal contributions are quite expected.

Some slightly surprising findings reported here should however be discussed, like the failure to identify any frontal source with EEG, at the MMN latency. A careful inspection of the MMN literature reveals that it is indeed not straightforward to detect IFG activation from EEG responses, unless one considers specific priors with discrete ECD models (Jemel et al., 2002; MacLean et al., 2015; Rissling et al., 2014). However, two studies using distributed source models did report a contribution from IFG (Fulham et al., 2014; in a language study: Hanna, 2014). In our case, it is likely that inferior frontal activations were less plausible (possibly weaker) than supra-temporal ones, and as such they have been discarded by MSP, which incorporates a

sparsity constraint. It should also be noted that few MEG studies also succeeded in localizing these regions (Lappe et al., 2013b; Recasens et al., 2015).

Another unexpected result pertains to the contribution of the left middle occipital gyrus and the right inferior temporal gyrus for intensity deviance with fused inversion. It is worth recalling that the intensity MMN was not significant at the scalp-level over the time interval between 100 and 150 ms. We therefore assume that these sources are false positive. Finally, frontal contributions were located in the very posterior part of the IFG, just above supratemporal regions. However, the fact that we observed activations in IFG but not in PP (rising edge of the MMN, INT) and in HG but not in IFG (peak of the MMN, INT) allows to reject the hypothesis of two mis-localized and correlated clusters of opposite sign.

Conclusion

This paper develops an evaluation procedure to assess the benefit of fusing EEG and MEG data for distributed source localization. Critically, it offers a generic approach that is applicable to empirical data. It thus paves the way to go beyond simulations to evaluate the gain in performance afforded by multimodal integration. Importantly, this assessment is data dependent. This means that one could assess the relative importance of combining EEG and MEG recordings, for a given cortical network (e.g. associated with a particular type of perception or cognitive tasks) and a given population of subjects (e.g. with more or less heterogeneity). In the present example of studying auditory mismatch responses, multimodal integration proved to outperform unimodal inference, as expected, and can now be highly advised for future studies in the field. We could indeed identify a bilateral fronto-temporal network for both frequency and intensity deviance responses which is in accordance with the existing literature. Promisingly, the spatial resolution reached with fused inversion allowed a detailed spatio-temporal description within the supratemporal plane. These findings should however be balanced against the experimental cost of simultaneous EEG-MEG acquisitions that remain somewhat less straightforward that unimodal ones. The detailed auditory network reconstructed here represents a crucial step for future studies that will aim at addressing the fine neurophysiological and computational mechanisms underlying auditory processing.

Acknowledgments

We thank Sébastien Daligault and Pascal Calvat for programming support in interfacing with the CC IN2P3. We acknowledge CC-IN2P3 for providing computing resources and services needed for this work. We thank Emmanuel Maby and Gaëtan Sanchez for helpful discussions. We would also like to thank the three anonymous reviewers for their helpful comments and suggestions. This work was supported by a grant from the Agence Nationale de la Recherche of the French Ministry of Research ANR-11-BSH2-001-01 to AC and FL and a grant from the Fondation pour la Recherche Médicale (FRM) to OB and JM. This work was conducted in the framework of the LabEx CeLyA ("Centre Lyonnais d'Acoustique", ANR-10-LABX-0060) and of the LabEx Cortex ("Construction, Function and Cognitive Function and Rehabilitation of the Cortex", ANR-10-LABX-0042) of Université de Lyon, within the program "Investissements d'avenir" (ANR-11- IDEX-0007) operated by the French National Research Agency (ANR).

Appendix. The Free Energy approximation

Variational Bayes (VB) enables a simultaneous twofold inference, on models and model parameters, respectively (Beal, 2003; Starke and Ostwald, 2017). The former rests on an approximation to the model log-evidence (the variational free-energy), and the latter is provided by the (Laplace approximate) variational posterior distribution. Denoted by F and given the model M with parameters θ, the variational free-energy is such that:

$$\log \mathrm{p}(\mathrm{Y}|\mathrm{M}) = \mathrm{F}(\mathrm{M}) + \mathrm{KL}[\mathrm{q}(\theta), \mathrm{p}(\theta|\mathrm{Y}, \mathrm{M})] \quad \text{(A.1)}$$

The left hand term corresponds to the model Log-evidence and $\mathrm{q}(\theta)$ indicates the variational posterior distribution which is updated to maximize free energy and approximate the true posterior $\mathrm{p}(\theta|\mathrm{Y}, \mathrm{M})$. KL is the Kullback Leibler divergence and measures the discrepancy between any two probability densities. It writes:

$$\mathrm{KL}[q(\theta), p(\theta|Y, M)] = \int q(\theta) \log \frac{q(\theta)}{p(\theta|Y, M)} \quad \text{(A.2)}$$

Importantly, KL equals zero when the two densities are equal, and is greater than zero otherwise. This means that the free energy is a lower bound to the log-evidence. Variational inference consists in updating $q(\theta)$ to maximize free energy so that, at convergence

$$q(\theta) \approx p(\theta|Y, M) \quad \text{(A.3)}$$
$$F(M) \approx \log p(Y|M)$$

As an approximate to model evidence, F can be used for model comparison and selection (Penny et al., 2007). Interestingly, it can be rewritten as follows:

$$F(M) = \int q(\theta) \log p(Y|\theta, M)\, d\theta - \mathrm{KL}[q(\theta), p(\theta)] \quad \text{(A.4)}$$

The first term on the right hand side is an accuracy term, the marginal log likelihood. The second term is a complexity (penalty) term, the KL divergence between the variational and the prior. An important aspect disclosed by this formulation is that letting $q(\theta)$ departing from prior $p(\theta)$, which happens if data Y is not fully compatible with prior $p(\theta)$, increases model complexity and should thereby be compensated by a better fit of data Y (a larger accuracy) in order to maximize $F(M)$.

Variational free-energy affords an approximation to the log Bayes Factor introduced by Kass and Raftery (1995) to compare two models based on their relative log-evidence after confrontation to the same data Y. Given equation A.3, the log Bayes Factor for model M_i with respect to model M_j writes as follows:

$$\log BF_{i,j} = \log \frac{p(Y|M_i)}{p(Y|M_j)} \approx F(M_i) - F(M_j) \quad \text{(A.5)}$$

This approximation enters the general Bayesian Model Comparison (BMC) to select the most plausible model among several candidates, which is central to the proposed evaluation scheme where model space comprises three group prior models ($\{M_{EEG}, M_{MEG}, M_{Fusion}\}$).

In the context of models for neuroimaging data, the variational free-energy has shown to surpass other common approximate metrics for model comparison, namely the Akaike's Information Criterion (AIC) and the Bayesian information criterion (BIC) (Penny, 2012). Furthermore, it has been validated against exact but computationally prohibitive Monte-Carlo estimates of the log-evidence (Friston et al., 2007). It can be used to compute Bayes factors, model posteriors and model exceedance probabilities.

CRediT Author Statement

Conceptualization, AC, FL and JM; Methodology, FL and JM; Software, FL and JM; Investigation, AC and FL; Writing, AC, FL and JM; Funding Acquisition, OB, AC and JM; Supervision, OB, AC and JM.

Declaration of Interest

The authors declare that they have no conflict of interests.

Ethic Statement

The authors state that written informed consent was obtained from participants. Ethical approval was obtained from the appropriate regional ethics committee on Human Research (CPP Sud-Est IV - 2010-A00301-38).

.Data and Code Availability Statement

The data and code that support the findings of this study are available from the corresponding author upon request.

REFERENCES

Andreou, L.-V., Griffiths, T.D., Chait, M., 2015. Sensitivity to the temporal structure of rapid sound sequences — An MEG study. NeuroImage 110, 194–204. doi:10.1016/j.neuroimage.2015.01.052

Auksztulewicz, R., Friston, K., 2016. Repetition suppression and its contextual determinants in predictive coding. CORTEX. doi:10.1016/j.cortex.2015.11.024

Auksztulewicz, R., Friston, K., 2015. Attentional Enhancement of Auditory Mismatch Responses: a DCM/MEG Study. Cerebral Cortex. doi:10.1093/cercor/bhu323

Babiloni, C., Carducci, F., Romani, G.L., Rossini, P.M., Angelone, L.M., Cincotti, F., 2004. Multimodal integration of EEG and MEG data: A simulation study with variable signal-to-noise ratio and number of sensors. Hum. Brain Mapp. 22, 52–62. doi:10.1002/hbm.20011

Babiloni, C., Pizzella, V., Gratta, C.D., Ferretti, A., Romani, G.L., 2009. Chapter 5 Fundamentals of Electroencefalography, Magnetoencefalography, and Functional Magnetic Resonance Imaging, in: International Review of Neurobiology. Elsevier, pp. 67–80. doi:10.1016/S0074-7742(09)86005-4

Baillet, S., Garnero, L., Marin, G., Hugonin, J.P., 1999. Combined MEG and EEG source imaging by minimization of mutual information. IEEE Trans Biomed Eng 46, 522–534.

Beal, M., 2003. VARIATIONAL ALGORITHMS FOR APPROXIMATE BAYESIAN INFERENCE.

Carbajal, G.V., Malmierca, M.S., 2018. The Neuronal Basis of Predictive Coding Along the Auditory Pathway: From the Subcortical Roots to Cortical Deviance Detection. Trends in Hearing 22, 2331216518784822. doi:10.1177/2331216518784822

Chowdhury, R.A., Zerouali, Y., Hedrich, T., Heers, M., Kobayashi, E., Lina, J.-M., Grova, C., 2015. MEG-EEG Information Fusion and Electromagnetic Source Imaging: From Theory to Clinical Application in Epilepsy. Brain Topogr 28, 785–812. doi:10.1007/s10548-015-0437-3

Cohen, D., Cuffin, B.N., 1987. A method for combining MEG and EEG to determine the sources. Phys Med Biol 32, 85–89.

Dale, A.M., Sereno, M.I., 1993. Improved Localization of Cortical Activity bu Combining EEG and MEG with MRI Cortical Surface Reconstruction : A Linear Approach. J Cogn Neurosci 5, 162–176.

Daunizeau, J., Grova, C., Mattout, J., Marrelec, G., Clonda, D., Goulard, B., Pélégrini-Issac, M., Lina, J.M., Benali, H., 2005. Assessing the relevance of fMRI-based prior in the EEG inverse problem: a bayesian model comparison approach. IEEE Trans. Signal Process. 53, 3461–3472. doi:10.1109/TSP.2005.853220

Deouell, L.Y., 2007. The Frontal Generator of the Mismatch Negativity Revisited. Journal of Psychophysiology 21, 188–203. doi:10.1027/0269-8803.21.3.188

Escera, C., Leung, S., Grimm, S., 2014. Deviance detection based on regularity encoding along the auditory hierarchy: electrophysiological evidence in humans. Brain Topogr 27, 527–538. doi:10.1007/s10548-013-0328-4

Escera, C., Malmierca, M.S., 2014. The auditory novelty system: an attempt to integrate human and animal research. Psychophysiology 51, 111–123. doi:10.1111/psyp.12156

Friston, K., 2005. A theory of cortical responses. Philosophical Transactions of the Royal Society B: Biological Sciences 360, 815–836. doi:10.1098/rstb.2005.1622

1143 Friston, K., Chu, C., Mourão-Miranda, J., Hulme, O., Rees, G., Penny, W.D.,
1144 Ashburner, J., 2008a. Bayesian decoding of brain images. NeuroImage 39, 181–
1145 205. doi:10.1016/j.neuroimage.2007.08.013
1146 Friston, K., Harrison, L., Daunizeau, J., Kiebel, S., Phillips, C., Trujillo-Barreto, N.,
1147 Henson, R., Flandin, G., Mattout, J., 2008b. Multiple sparse priors for the M/EEG
1148 inverse problem. NeuroImage 39, 1104–1120.
1149 doi:10.1016/j.neuroimage.2007.09.048
1150 Friston, K., Henson, R., Phillips, C., Mattout, J., 2006a. Bayesian estimation of
1151 evoked and induced responses. Hum. Brain Mapp. 27, 722–735.
1152 doi:10.1002/hbm.20214
1153 Friston, K., Henson, R., Phillips, C., Mattout, J., 2006b. Bayesian estimation of
1154 evoked and induced responses. Hum. Brain Mapp. 27, 722–735.
1155 doi:10.1002/hbm.20214
1156 Friston, K., Mattout, J., Trujillo-Barreto, N., Ashburner, J., Penny, W.D., 2007.
1157 Variational free energy and the Laplace approximation. NeuroImage 34, 220–234.
1158 doi:10.1016/j.neuroimage.2006.08.035
1159 Fuchs, M., Wagner, M., Wischmann, H.A., Köhler, T., Theissen, A., Drenckhahn, R.,
1160 Buchner, H., 1998. Improving source reconstructions by combining bioelectric
1161 and biomagnetic data. Electroencephalogr Clin Neurophysiol 107, 93–111.
1162 Fulham, W.R., Michie, P.T., Ward, P.B., Rasser, P.E., Todd, J., Johnston, P.J.,
1163 Thompson, P.M., Schall, U., 2014. Mismatch negativity in recent-onset and
1164 chronic schizophrenia: a current source density analysis. PLoS ONE 9, e100221.
1165 doi:10.1371/journal.pone.0100221
1166 Giard, M.H., Lavikahen, J., Reinikainen, K., Pessiglione, M., Bertrand, O., Pernier, J.,
1167 Näätänen, R., 1995. Separate representation of stimulus frequency, intensity,
1168 and duration in auditory sensory memory: an event-related potential and dipole-
1169 model analysis. J Cogn Neurosci 7, 133–143. doi:10.1162/jocn.1995.7.2.133
1170 Gramfort, A., Papadopoulo, T., Olivi, E., Clerc, M., 2010. OpenMEEG: opensource
1171 software for quasistatic bioelectromagnetics. Biomed Eng Online 9, 45.
1172 doi:10.1186/1475-925X-9-45
1173 Hanna, J., 2014. Neurophysiological evidence for whole form retrieval of complex
1174 derived words: a mismatch negativity study 1–13.
1175 doi:10.3389/fnhum.2014.00886/abstract
1176 Hämäläinen, M.S., Sarvas, J., 1989. Realistic conductivity geometry model of the
1177 human head for interpretation of neuromagnetic data. IEEE Trans Biomed Eng
1178 36, 165–171. doi:10.1109/10.16463
1179 Henson, R., Flandin, G., Friston, K., Mattout, J., 2010. A parametric empirical
1180 Bayesian framework for fMRI-constrained MEG/EEG source reconstruction. Hum.
1181 Brain Mapp. 31, 1512–1531. doi:10.1002/hbm.20956
1182 Henson, R., Mouchlianitis, E., Friston, K., 2009. MEG and EEG data fusion:
1183 simultaneous localisation of face-evoked responses. NeuroImage 47, 581–589.
1184 doi:10.1016/j.neuroimage.2009.04.063
1185 Henson, R., Wakeman, D.G., Litvak, V., Friston, K., 2011. A Parametric Empirical
1186 Bayesian Framework for the EEG/MEG Inverse Problem: Generative Models for
1187 Multi-Subject and Multi-Modal Integration. Front Hum Neurosci 5, 76.
1188 doi:10.3389/fnhum.2011.00076
1189 Huotilainen, M., Winkler, I., Alho, K., Escera, C., Virtanen, J., Ilmoniemi, R.J.,
1190 Jääskeläinen, I.P., Pekkonen, E., Näätänen, R., 1998. Combined mapping of
1191 human auditory EEG and MEG responses. Electroencephalogr Clin Neurophysiol
1192 108, 370–379.

Jemel, B., Achenbach, C., Müller, B.W., Röpcke, B., Oades, R.D., 2002. Mismatch negativity results from bilateral asymmetric dipole sources in the frontal and temporal lobes. Brain Topogr 15, 13–27.
Kass, R., Raftery, A.E., 1995. Bayes Factor. Journal of the American Statistical Association 90, 773–795.
Kuuluvainen, S., Nevalainen, P., Sorokin, A., Mittag, M., Partanen, E., Putkinen, V., Seppänen, M., Kähkönen, S., Kujala, T., 2014. The neural basis of sublexical speech and corresponding nonspeech processing: A combined EEGâ€“MEG study. Brain and Language 130, 19–32. doi:10.1016/j.bandl.2014.01.008
Lappe, C., Steinsträter, O., Pantev, C., 2013a. Rhythmic and melodic deviations in musical sequences recruit different cortical areas for mismatch detection. Front Hum Neurosci 7, 260. doi:10.3389/fnhum.2013.00260
Lappe, C., Steinsträter, O., Pantev, C., 2013b. A beamformer analysis of MEG data reveals frontal generators of the musically elicited mismatch negativity. PLoS ONE 8, e61296. doi:10.1371/journal.pone.0061296
Lecaignard, F., Bertrand, O., Gimenez, G., Mattout, J., Caclin, A., 2015. Implicit learning of predictable sound sequences modulates human brain responses at different levels of the auditory hierarchy. Front Hum Neurosci 9, 505. doi:10.3389/fnhum.2015.00505
Lecaignard, F., Mattout, J., 2015. Forward Models for EEG/MEG, in: Toga, A.W. (Ed.), Brain Mapping. Elsevier Academic Press, pp. 549–555.
Levänen, S., Ahonen, A., Hari, R., McEvoy, L., Sams, M., 1996. Deviant auditory stimuli activate human left and right auditory cortex differently. Cerebral Cortex 6, 288–296.
Liégeois-Chauvel, C., Musolino, A., Badier, J.-M., Marquis, P., Chauvel, P., 1994. Evoked potentials recorded from the auditory cortex in man: evaluation and topography of the middle latency components. Electroencephalogr Clin Neurophysiol 92, 204–214.
Litvak, V., Friston, K., 2008. Electromagnetic source reconstruction for group studies. NeuroImage 42, 1490–1498. doi:10.1016/j.neuroimage.2008.06.022
Litvak, V., Jafarian, A., Zeidman, P., Tibon, R., Henson, R., Friston, K., 2019. There's no such thing as a "true" model: the challenge of assessing face validity*, in:. Presented at the 2019 IEEE International Conference on Systems, Man and Cybernetics (SMC), IEEE, pp. 4403–4408. doi:10.1109/SMC.2019.8914255
Lopes da Silva, F., 2013. EEG and MEG: relevance to neuroscience. Neuron 80, 1112–1128. doi:10.1016/j.neuron.2013.10.017
MacLean, S.E., Blundon, E.G., Ward, L.M., 2015. Brain regional networks active during the mismatch negativity vary with paradigm. Neuropsychologia 75, 242–251. doi:10.1016/j.neuropsychologia.2015.06.019
Marco-Pallarés, J., Grau, C., Ruffini, G., 2005. Combined ICA-LORETA analysis of mismatch negativity 25, 471–477. doi:10.1016/j.neuroimage.2004.11.028
Mattout, J., Garnero, L., Pélégrini-Issac, M., Benali, H., 2005. Multivariate source prelocalization (MSP): use of functionally informed basis functions for better conditioning the MEG inverse problem. 26, 356–373. doi:10.1016/j.neuroimage.2005.01.026
Mattout, J., Henson, R., Friston, K., 2007. Canonical source reconstruction for MEG. Computational Intelligence and Neuroscience 67613. doi:10.1155/2007/67613
Mattout, J., Phillips, C., Penny, W.D., Rugg, M.D., Friston, K., 2006. MEG source localization under multiple constraints: an extended Bayesian framework. NeuroImage 30, 753–767. doi:10.1016/j.neuroimage.2005.10.037

1243 Molins, A., Hämäläinen, M.S., Stufflebeam, S., Brown, E.N., 2008. Quantification of
1244 the benefit from integrating MEG and EEG data in minimum l2-norm estimation
1245 42, 1069–1077. doi:10.1016/j.neuroimage.2008.05.064
1246 Morlet, D., Fischer, C., 2014. MMN and novelty P3 in coma and other altered states
1247 of consciousness: a review. Brain Topogr 27, 467–479. doi:10.1007/s10548-013-
1248 0335-5
1249 Näätänen, R., Kujala, T., Escera, C., Baldeweg, T., Kreegipuu, K., Carlson, S.,
1250 Ponton, C., 2012. The mismatch negativity (MMN)--a unique window to disturbed
1251 central auditory processing in ageing and different clinical conditions. Clin
1252 Neurophysiol 123, 424–458. doi:10.1016/j.clinph.2011.09.020
1253 Näätänen, R., Paavilainen, P., Rinne, T., Alho, K., 2007. The mismatch negativity
1254 (MMN) in basic research of central auditory processing: a review. Clin
1255 Neurophysiol 118, 2544–2590. doi:10.1016/j.clinph.2007.04.026
1256 Pantev, C., Bertrand, O., Eulitz, C., Verkindt, C., Hampson, S., Schuierer, G., Elbert,
1257 T., 1995. Specific tonotopic organizations of different areas of the human auditory
1258 cortex revealed by simultaneous magnetic and electric recordings.
1259 Electroencephalogr Clin Neurophysiol 94, 26–40.
1260 Penny, W.D., 2012. Comparing Dynamic Causal Models using AIC, BIC and Free
1261 Energy 59, 319–330. doi:10.1016/j.neuroimage.2011.07.039
1262 Penny, W.D., Mattout, J., Trujillo-Barreto, N., 2007. Bayesian model selection and
1263 averaging, in: Statistical Parametric Mapping. Elsevier, pp. 454–467.
1264 doi:10.1016/B978-012372560-8/50035-8
1265 Penny, W.D., Stephan, K.E., Daunizeau, J., Rosa, M.J., Friston, K., Schofield, T.M.,
1266 Leff, A.P., 2010. Comparing families of dynamic causal models. PLoS Comput
1267 Biol 6, e1000709. doi:10.1371/journal.pcbi.1000709
1268 Phillips, C., Mattout, J., Rugg, M.D., Maquet, P., Friston, K., 2005. An empirical
1269 Bayesian solution to the source reconstruction problem in EEG 24, 997–1011.
1270 doi:10.1016/j.neuroimage.2004.10.030
1271 Plonsey, R., Heppner, D.B., 1967. Considerations of quasi-stationarity in
1272 electrophysiological systems. Bull Math Biophys 29, 657–664.
1273 Poeppel, D., Hickok, G., 2015. Electromagnetic recording of the auditory system.
1274 Handb Clin Neurol 129, 245–255. doi:10.1016/B978-0-444-62630-1.00014-7
1275 Puce, A., Hämäläinen, M.S., 2017. A Review of Issues Related to Data Acquisition
1276 and Analysis in EEG/MEG Studies. Brain Sciences 7.
1277 doi:10.3390/brainsci7060058
1278 Recasens, M., Grimm, S., Capilla, A., Nowak, R., Escera, C., 2014a. Two sequential
1279 processes of change detection in hierarchically ordered areas of the human
1280 auditory cortex. Cereb Cortex 24, 143–153. doi:10.1093/cercor/bhs295
1281 Recasens, M., Grimm, S., Wollbrink, A., Pantev, C., Escera, C., 2014b. Encoding of
1282 nested levels of acoustic regularity in hierarchically organized areas of the human
1283 auditory cortex. Hum. Brain Mapp. 35, 5701–5716. doi:10.1002/hbm.22582
1284 Recasens, M., Leung, S., Grimm, S., Nowak, R., Escera, C., 2015. Repetition
1285 suppression and repetition enhancement underlie auditory memory-trace
1286 formation in the human brain: an MEG study. NeuroImage 108, 75–86.
1287 doi:10.1016/j.neuroimage.2014.12.031
1288 Rinne, T., Alho, K., Ilmoniemi, R.J., Virtanen, J., Näätänen, R., 2000. Separate time
1289 behaviors of the temporal and frontal mismatch negativity sources. NeuroImage
1290 12, 14–19. doi:10.1006/nimg.2000.0591

Rissling, A.J., Miyakoshi, M., Sugar, C.A., Braff, D.L., Makeig, S., Light, G.A., 2014. Cortical substrates and functional correlates of auditory deviance processing deficits in schizophrenia. YNICL 6, 424–437. doi:10.1016/j.nicl.2014.09.006

Ruhnau, P., Herrmann, B., Maess, B., Brauer, J., Friederici, A.D., Schröger, E., 2013. Processing of complex distracting sounds in school-aged children and adults: evidence from EEG and MEG data. Front Psychol 4, 717. doi:10.3389/fpsyg.2013.00717

Rush, S., Driscoll, D.A., 1968. Current distribution in the brain from surface electrodes. Anesth. Analg. 47, 717–723.

Schairer, K.S., Gould, H.J., Pousson, M.A., 2001. Source generators of mismatch negativity to multiple deviant stimulus types. Brain Topogr 14, 117–130.

Scherg, M., Vajsar, J., Picton, T.W., 1989. A Source Analysis of the Late Human Auditory Evoked Potentials. J Cogn Neurosci 1, 336–355.

Schönwiesner, M., Novitski, N., Pakarinen, S., Carlson, S., Tervaniemi, M., Näätänen, R., 2007. Heschl's gyrus, posterior superior temporal gyrus, and mid-ventrolateral prefrontal cortex have different roles in the detection of acoustic changes. Journal of Neurophysiology 97, 2075–2082. doi:10.1152/jn.01083.2006

Sharon, D., Hämäläinen, M.S., Tootell, R.B.H., Halgren, E., Belliveau, J.W., 2007. The advantage of combining MEG and EEG: comparison to fMRI in focally stimulated visual cortex 36, 1225–1235. doi:10.1016/j.neuroimage.2007.03.066

Starke, L., Ostwald, D., 2017. Variational Bayesian Parameter Estimation Techniques for the General Linear Model. Front Neurosci 11, 504. doi:10.3389/fnins.2017.00504

Stephan, K.E., Penny, W.D., Daunizeau, J., Moran, R., Friston, K., 2009. Bayesian model selection for group studies. NeuroImage 46, 1004–1017. doi:10.1016/j.neuroimage.2009.03.025

Sussman, E.S., Shafer, V.L., 2014. New Perspectives on the Mismatch Negativity (MMN) Component: An Evolving Tool in Cognitive Neuroscience. Brain Topogr 27, 425–427. doi:10.1007/s10548-014-0381-7

Vallaghé, S., Clerc, M., 2009. A global sensitivity analysis of three- and four-layer EEG conductivity models. IEEE Trans Biomed Eng 56, 988–995. doi:10.1109/TBME.2008.2009315

Waberski, T.D., Kreitschmann-Andermahr, I., Kawohl, W., Darvas, F., Ryang, Y., Rodewald, M., Gobbelé, R., Buchner, H., 2001. Spatio-temporal source imaging reveals subcomponents of the human auditory mismatch negativity in the cingulum and right inferior temporal gyrus. Neurosci Lett 308, 107–110.

Yvert, B., Fischer, C., Guénot, M., Krolak-Salmon, P., Isnard, J., Pernier, J., 2002. Simultaneous intracerebral EEG recordings of early auditory thalamic and cortical activity in human. Eur J Neurosci 16, 1146–1150. doi:10.1046/j.1460-9568.2002.02162.x